Mineralogy and Petrology (2022) 116:229–249
https://doi.org/10.1007/s00710-022-00774-2

ORIGINAL PAPER

Estimation of Li and OH contents in (Li,Al)-bearing tourmalines from Raman spectra

Adam Pieczka[1] · Bożena Gołębiowska[1] · Marcin Stachowicz[2] · Krzysztof Nejbert[2] · Jakub Kotowski[2] · Piotr Jeleń[3] · Andreas Ertl[4] · Krzysztof Woźniak[5]

Received: 2 June 2021 / Accepted: 27 January 2022 / Published online: 4 April 2022

Abstract

Six Al- and Li-bearing tourmaline crystals from pegmatites were structurally and chemically characterized. These samples can be assigned to elbaite, fluor-elbaite and rossmanite. Quantitative analyses of light elements such as Li, B and H are not always easily accessible. Therefore a method for the calculation of Li and OH would be of a general interest for the Geosciences. In the present work we test whether relatively accurate Li and OH estimations are possible based on the deconvolution of the O–H stretching vibration modes in a Raman spectrum on common (Al,Li)-rich tourmalines. We use the short-range arrangement model in our band interpretation as this model, in contrast to other models, provides the ability to evaluate an additional parameter by analyzing the OH stretching modes that can be used in the formula calculation process, which ultimately leads to the estimation of Li and OH with high accuracy. We also compare microprobe and Raman spectroscopy results, which we combine, with optimized data derived from microprobe and single-crystal structure refinement by using the same crystals. Based on our investigations, where the Raman spectra were recorded on non-oriented crystal sections, we conclude that we produce more accurate estimations, when the effects of the section orientation are considered. Therefore, we also propose a new method to correct the influence of the orientation of the crystal section.

Keywords (Al,Li)-bearing tourmalines · Lithium content · Hydroxyl content · Structure refinement · Raman spectroscopy · OH stretching vibrations

Introduction

The tourmaline supergroup comprises an abundant set of cyclic borosilicates with compositions corresponding to the generic formula $XY_3Z_6(T_6O_{18})(BO_3)_3V_3W$, where the symbols X, Y, Z, T, B, V and W denote different structural sites beside those occupied only by oxygen (Henry et al. 2011). The sites are occupied by:

^{IX}X – Na^+, K^+, Ca^{2+}, Pb^{2+}, or is vacant (□)
^{VI}Y – Fe^{2+}, Mg^{2+}, Mn^{2+}, Al^{3+}, Li^+, Fe^{3+}, Cr^{3+}, V^{3+}, Ti^{4+}, Zn^{2+}, Cu^{2+}, Ni^{2+}, □, …
^{VI}Z – Al^{3+}, Fe^{3+}, Cr^{3+}, V^{3+}, Mg^{2+}, Fe^{2+}, …
^{IV}T – Si^{4+}, Al^{3+}, B^{3+}
^{III}B – B^{3+}
^{III}V – OH^-, O^{2-}
^{III}W – OH^-, F^-, O^{2-}

The members of this mineral supergroup crystallize in the rhombohedral *R*3*m* space group. The presence of five non-equivalent cationic sites (X, Y, Z, T, B), and two anionic sites, V and W, occupied by varying monovalent (OH^- and $OH^- \pm F^-$, respectively) and divalent O^{2-} anions, results in a large number of compositional combinations, 33 of which to date have been confirmed in natural tourmaline crystals and approved as valid mineral species of the supergroup (Bosi

Editorial handling: L. Nasdala

✉ Adam Pieczka
pieczka@agh.edu.pl

[1] Department of Mineralogy, Petrography and Geochemistry, AGH University of Science and Technology, Mickiewicza 30, 30-059 Kraków, Poland

[2] Faculty of Geology, University of Warsaw, Żwirki and Wigury 93, 02-089 Warszawa, Poland

[3] Faculty of Materials Science and Ceramics, AGH University of Science and Technology, Mickiewicza 30, 30-059 Kraków, Poland

[4] Institut Für Mineralogie Und Kristallographie, Geozentrum, Universität Wien, Althanstrasse 14, 1090 Wien, Austria

[5] Department of Chemistry, University of Warsaw, Pasteura 1, 02-093 Warszawa, Poland

2018). Lithium-bearing tourmalines exist within this group as species in which Al and Li are the only Y-site occupants. This particular subgroup contains five approved minerals and four hypothetical members still not found in nature as dominant species (Table 1). Of course, compositions of natural crystals are more complex because they always display an isomorphic solid solution of Al-Li end-members with other Li-free end-members existing in the supergroup. Therefore, in Table 1 the end-members olenite (Sokolov et al. 1986), alumino-oxy-rossmanite (Ertl et al. 2022) and hypothetical B-analogue of alumino-oxy-rossmanite are also presented, i.e., the three additional Al-rich end-members which can participate in the formation of (Al,Li)-tourmaline chemistry. All crystals containing Li, which still cannot be measured by conventional electron-probe microanalysis (EPMA), cause additional analytical difficulty due to Li_2O determination. Such samples require special measuring techniques, e.g., laser ablation inductively coupled plasma mass spectrometry (LA-ICP-MS), secondary ion mass spectrometry (SIMS), laser induced breakdown spectroscopy (LIBS), single-crystal X-ray diffraction and structure refinement (SREF), or others, usually not available in some research units (e.g., Dyar et al. 1998; Ertl et al. 2003, 2012; Roda-Robles et al. 2015). Therefore, in practice, light elements such as Li, B, and H are commonly just estimated on the basis of the tourmaline-supergroup stoichiometry.

Henry et al. (2011) briefly characterized in Appendix 5 normalization procedures and estimation of light elements, including Li and H, and oxidation states of elements on the basis of analytical data obtained by the use of EPMA, currently most widely used for analyzing the chemical composition of minerals. These authors recommended three normalization procedures for the crystal-chemical and structural formulae: (1) on fixed total number of anions O + OH + F = 31, or another modified content of anions resulted from additional assumptions, e.g., the presence of B at the amount of 3 atoms per formula unit (apfu); (2) on 15 (Y + Z + T) cations, which was recommended for tourmalines with low Li contents and minor B at the T site; and (3) on fixed Si content equal to 6 apfu, which is usually employed for (Al,Li)-bearing tourmalines. Each of these procedures provide estimations of light elements and oxidation states of transition elements by introduction additional compositional constraints on the atomic scale, e.g., F + OH = 4, Li = 15 – $(Y + Z + T)_{EPMA}$, or others. However, each of the recommended normalization procedures may introduce significant inaccuracies in the calculated formulae. For instance, the procedure (3) recommended for (Al,Li)-tourmalines neglects an often occurring Si deficiency, which must be completed by Al ± B excess. As a result the remaining components will be overestimated and the Li content underestimated. The same procedure causes in the case of an overestimated Si content due to EPMA inaccuracy or the presence of quartz or other silicate micro- to nano-inclusions in the analytical spot an underestimation of the remaining components, while the Li content will be overestimated. The analytical inaccuracy of the SiO_2 determination in the range of ~1–2% relative, as typical for EPMA analysis of lighter elements, would be ~0.3–0.7 wt% SiO_2, corresponding to ≥ 0.1 Si apfu for a value of ~37 wt% SiO_2, a content typical for tourmalines. Thus, it is clear that such 'calculating' procedures can lead to crystal-chemical and structural tourmaline formulae that sometimes inaccurately reflect the actual compositions.

Pesquera et al. (2016) proposed a multiple regression equation evaluated on the basis of almost 300 tourmaline analyses selected from literature with Li measured directly, for estimation of Li in tourmaline from electron microprobe determinations: Li_2O (in wt%) = 2.356 + 0.124 SiO_2 – 0.121 Al_2O_3 – 0.178 FeO_{total} – 0.162 MnO. For the selected set of analyses they obtained a better correlation between analyzed

Table 1 Al- and Al,Li-tourmalines (approved and hypothetical[1])

Approved mineral name	Chemical name	End-member formula
Olenite	Olenite	$NaAl_3Al_6(Si_6O_{18})(BO_3)_3O_3OH$
Alumino-oxy-rossmanite	Alumino-oxy-rossmanite	$\square Al_3Al_6(Si_5AlO_{18})(BO_3)_3(OH)_3O$
	B-analogue of alumino-oxy-rossmanite	$\square Al_3Al_6(Si_5BO_{18})(BO_3)_3(OH)_3O$
Rossmanite	Rossmanite	$\square(LiAl_2)Al_6(Si_6O_{18})(BO_3)_3(OH)_3(OH)$
	Fluor-rossmanite	$\square(LiAl_2)Al_6(Si_6O_{18})(BO_3)_3(OH)_3F$
	Oxy-rossmanite	$\square(Li_{0.5}Al_{2.5})Al_6(Si_6O_{18})(BO_3)_3(OH)_3O$
Elbaite	Elbaite	$Na(Li_{1.5}Al_{1.5})Al_6(Si_6O_{18})(BO_3)_3(OH)_3(OH)$
Fluor-elbaite	Fluor-elbaite	$Na(Li_{1.5}Al_{1.5})Al_6(Si_6O_{18})(BO_3)_3(OH)_3F$
Darrellhenryite	Oxy-elbaite	$Na(LiAl_2)Al_6(Si_6O_{18})(BO_3)_3(OH)_3O$
	Liddicoatite	$Ca(Li_2Al)Al_6(Si_6O_{18})(BO_3)_3(OH)_3OH$
Fluor-liddicoatite	Fluor-liddicoatite	$Ca(Li_2Al)Al_6(Si_6O_{18})(BO_3)_3(OH)_3F$
	Oxy-liddicoatite	$Ca(Li_{1.5}Al_{1.5})Al_6(Si_6O_{18})(BO_3)_3(OH)_3O$

[1]Hypothetical species are marked with italic character

and calculated Li_2O content by using their proposed equation ($r^2 = 0.95$) than by using equation Li (apfu) = 15 – (Y + Z + T), considering the assumption (OH + F) = 4 pfu ($r^2 = 0.79$). Although the equation proposed by Pesquera et al. (2016) works well for many typical compositions of (Al,Li)-bearing tourmalines, Pieczka et al. (2018) noticed that it gives not very accurate results when a tourmaline is enriched in atypical components, e.g., ZnO. This is not surprising, because their equation neither includes the variable ZnO, nor some other compositional variables important for (Al,Li)-bearing tourmalines. Additionally, in spite of the good correlation, Fig. 3a presented in the original paper by Pesquera et al. (2016) shows significant differences between the Li_2O contents predicted by using their equation and the analytical values. The data are scattered in such a way that the predicted value may still differ from the actual Li_2O content by ≤ 0.5 wt%. This can be particularly problematic for low (Al,Li)-tourmalines, where the predicted Li content could lead to an overestimation of more than an order of magnitude.

These problems, including the difficult Li_2O analysis, were the main reasons for developing a new method of Li evaluation, which would feature high selectivity and accuracy, and simultaneously would be commonly accessible in every mineralogical laboratory. Relatively accurate Li and OH estimations are possible on the basis of deconvolution of the O–H stretching vibration modes in a Raman spectrum of (Al,Li)-bearing tourmalines as was shown by Pieczka et al. (2020). They used Zn-rich fluor-elbaite from Piława Górna, Lower Silesia, Poland, in their study. The results obtained by using two independent techniques: (1) based only on Raman spectroscopy (RS) and deconvolution of the recorded Raman spectrum of O–H stretching modes, (2) by direct formula calculation based on the EPMA results using an additional composition parameter derived from the deconvoluted Raman spectrum (EPMA + RS), were comparable with the results optimized on the basis of electron-probe microanalysis and structure refinement (EPMA + SREF). Differences of the Li and OH determination in both techniques were less than 0.06 Li apfu and ~0.1 OH apfu.

In the present work we test the EPMA + RS technique, which is easier to use and which gives more accurate results, on several crystals of common (Al,Li)-bearing tourmalines (elbaite, fluor-elbaite, rossmanite), especially taking into account the effects of the section orientation. We also compare the EPMA + RS results of the calculated formula with data derived from EPMA + SREF by using the same crystals. This study aims to verify whether the agreement of EPMA + SREF and EPMA + RS, as observed for the Zn-rich fluor-elbaite, is of a universal nature. If so, this technique would provide a relatively simple and fast tool for determining Li_2O and H_2O levels in natural tourmalines even in medium-equipped scientific units as Raman spectroscopy, which is currently widely available.

Material and methods

Materials

Six crystals of (Al,Li)-tourmalines, which represent mainly members of the elbaite – fluor-elbaite series, were selected for the studies. Two of bicolour tourmaline crystals (P2, P3) originated from the Julianna pegmatitic system (exposed in the period 2008–2011) from an amphibolite and migmatite quarry (DSS S.A Company) at Piława Górna, Lower Silesia, Poland (Szuszkiewicz et al. 2013). The WOLP, SS4, MOZ24 and BUX tourmalines are grains from crystals that were described previously (Ertl et al. 2009, 2010, 2013). They were re-examined using EPMA, RS and SREF using the same single crystal to rule out inaccuracies due to possible zoning. The analyses were performed on grains of the tourmaline crystals mounted in epoxy on glass plates that were grinded up to the thickness of ~0.2 mm, polished and coated with carbon. The grains of WOLP, SS4 and MOZ24 tourmaline had the cross-section sizes <1 mm; BUX tourmaline ~3 × 3 mm; bicolour tourmaline P2 represented a section of a trigonal crystal with ~3 cm diameter, with a pinkish rim of ~3 mm in thickness, and intensively green core; and P3 tourmaline was a fragment of another crystal of the same type with a thin pinkish rim of ~1 mm in thickness and a greenish core. Brief characteristics of these tourmalines are presented in Table 2.

Electron probe microanalysis and formula normalization procedure

Electron-probe microanalyses of the studied (Al,Li)-bearing tourmalines, performed in ~300 × 300 µm areas with a CAMECA SX 100 electron probe micro-analyser indicate homogeneous compositions. For each tourmaline studied, micro-Raman spectra were collected, and eventually a fragment of tourmaline was extracted from the area for single-crystal X-ray diffraction. The electron probe micro-analyser operated in wavelength-dispersive X-ray spectrometry (WDS) mode under the following conditions: accelerating voltage of 15 kV, beam current of 10 nA, beam diameter of 2 µm, peak count-time of 20 s, background time of 10 s before and 10 s after the peak. The following calibrant materials were used (the respective X-ray lines, diffracting crystals and mean detection limits in wt% element are quoted postpositioned in brackets): fluorophlogopite (F–*K*α, PC0, 0.12), albite (Na–*K*α, TAP, 0.03), diopside (Mg–*K*α, TAP, 0.02; Si–*K*α, TAP, 0.03; Ca–*K*α, PET, 0.02), orthoclase (Al–*K*α, TAP, 0.03; K–*K*α, PET, 0.02), rutile (Ti–*K*α, LPET, 0.02), rhodonite (Mn–*K*α, LIF, 0.09), hematite (Fe–*K*α, LIF, 0.08), V_2O_5 (V–*K*α, LIF, 0.06), Cr_2O_3 (Cr–*K*α, LPET, 0.02) and sphalerite (Zn–*K*α, LIF, 0.09). The raw data were reduced with the PAP routine of Pouchou and Pichoir (1991).

Table 2 Basic data on the studied tourmalines

Sample symbol	Occurence	Mineral name	Colour	Reference
SS4	Himalaya Mine, CA, U.S.A	elbaite	pale pink	Ertl et al. (2010)
MOZ24	Alto Ligonia, Mozambique	elbaite (Cu)	pale pink	Ertl et al. (2013)
BUX	Momeik, Myanmar	elbaite	pink	this study
WOLP	Wolkenburg, Germany	rossmanite	pink	Ertl et al. (2009)
P2-core	Piława Górna, Poland	elbaite	yellowish green	this study
P2-rim	Piława Górna, Poland	fluor-elbaite	pink	this study
P3-core	Piława Górna, Poland	elbaite	yellowish green	this study
P3-rim	Piława Górna, Poland	fluor-elbaite	pink	this study
Zn	Piława Górna, Poland	fluor-elbaite	pale greenish	Pieczka et al. (2020)

The atomic contents and chemical formulae of the tourmalines were normalized by two-step conditional procedure. The first-step normalization was done in relation to 14.5 (O, OH, F) anions pfu, i.e., 31 (O, OH, F) – 12 O – 4.5 O after assumption the presence of 6 Si and 3 B apfu, the total Fe as FeO, and the sum of Y-site occupants equal to 3 apfu. Li_2O and H_2O were calculated two different methods:

(i) based on the refined Y-site scattering (^{Y}s.s.) and <T–O> mean bond length (m.b.l.) in the EPMA + SREF formula,
(ii) based on the ^{Y}Al / $^{V+W}$OH ratio constrained to the $^{VOH}I_{YAlZAlZAl}$ / ($^{VOH}I_{YZZ}$ + $^{WOH}I_{YYY}$) parameter derived from Raman spectrum in the EPMA + RS formula.

When, as a result of such a normalization, an excess of Si > 6 apfu appeared (SiO_2 measured by EPMA), the "excess" Si was considered as an inaccuracy of the SiO_2 analysis or as external admixture of a silicate mineral. When the normalization was leading to Si < 6 apfu, the second-step normalization was done in relation to: (1) 26.5 (O, OH, F) anions pfu, i.e., 31 (O, OH, F) – 4.5 O under assumption of stoichiometric 3 B apfu and other conditions mentioned above, i.e., with Si deficiency only filled up by Al, or (2) 31 (O, OH, F) with B_2O_3, Li_2O and H_2O amounts matching the calculated B, Li and OH contents in the calculated formula to the refined Y-site electron density and <T–O> m.b.l. (EPMA + SREF), or to the $^{VOH}I_{YAlZAlZAl}$/ ($^{VOH}I_{YZZ}$ + $^{WOH}I_{YYY}$) parameter (EPMA + RS). When the studied tourmalines were originally described with not-fully occupied Y-site triplets (Ertl et al. 2009, 2010), some additional calculations were performed through decreasing of Li_2O amount and increasing H_2O in the used EPMA + RS procedure to obtain the value of the ^{Y}Al/$^{V+W}$OH parameter characteristic for the EPMA + SREF formula. Note, however, that such calculations are only possible if a structure refinement is made and structural parameters are known. Without the knowledge of the parameters, no calculation of EPMA + RS formula with not-fully occupied Y sites is possible. Thus, the covariations that describe the relationship between the Li_2O (Li) or H_2O (OH) contents and the ^{Y}Al / $^{V+W}$OH parameter, estimated by using EPMA + SREF and EPMA + RS procedures, were made only with the assumption of fully occupied octahedral sites (Y + Z = 9 apfu or Y = 3 apfu because Z = 6 Al apfu). This assumption is necessary because the real Y-site occupation is only known, when the actual Li_2O and H_2O contents of the studied crystal are known. If the contents of these light elements are not known, the crystal chemical tourmaline formula can only be calculated with the above assumption (Henry et al. 2011).

Single crystal X-ray structural studies and refinement procedure

X-ray data were collected using a SuperNova four-circle diffractometer equipped with an Eos charge-coupled device detector (Rigaku Oxford Diffraction), the detector-to-crystal distance was 45.8 mm. Mo$K\alpha$ radiation ($\lambda = 0.71073$ Å) was used at 50 kV and 0.8 mA. Crystals were attached either to a non-diffracting Mitegen micromount support or to a quartz glass fiber (0.01 mm diameter), which was glued to a glass capillary support. A frame-width of 1° in ω scans and frame times set to 30 s (sample P2c), 25 s (SS4), 15.2 s (BUX), 15 s (P2r and P3c), 12.5 s (MOZ and WOLP) and 5 s (P3r) were used for the studied crystals, respectively.

Crystal structures were solved with dual-space iterative phasing algorithm implemented in ShelXT (Sheldrick 2015a) that located all positions of cations (except hydrogen) and O anions. Correct element assignment for cations and anions was based upon compositional data obtained by EMPA and crystal-chemical reasoning, comprising site-scattering, coordination and bond lengths. In the Wyckoff notation the sites corresponding to symbols from generic formula have multiplicities of: X 3*a*; Y 9*b*; Z 18*c*; T 18*c*; B 9*b*; V 9*b*; W 3*a*. The model was refined with the least squares minimization using Shelxl (Sheldrick 2015b), within Olex2 (Dolomanov et al. 2009) as the graphical interface. When more than one element occupies the same position in the asymmetric unit, constraints for equal atom coordinates

and equal anisotropic displacement parameters for these groups of atoms within each unique site were applied. The occupancies of X, Y, T, W sites in all analyzed crystal structure models were refined. Site occupancies of Y and W were constrained to 1 and refined as Al vs Li and F vs O, respectively. The X site and T site were refined as fractional occupancies of ^{X}Na vs vacancy and ^{T}Si vs vacancy, respectively.

Raman spectroscopy (RS)

Unoriented Raman spectra of the studied (Li,Al)-tourmalines were collected in back-scattered geometry with a Horiba Labram HR spectrometer integrated with an Olympus BX 41 confocal microscope. The system was calibrated using the Rayleigh line. The spectra were recorded in the range of 50–4000 cm^{-1} using the 532 nm line of a solid-state Nd-YAG laser (10 mW) and 1800 grating, on randomly oriented sections of crystals mounted in epoxy resin that was used previously for EPMA and later was partly extracted for SREF studies. The only exception was a bicolour tourmaline (P3), for which Raman spectra were recorded on the sections prepared as $\parallel \mathbf{c}$ and $\perp \mathbf{c}$, to show difference in band intensities and their dependence on crystal section orientation. Prior to the Raman measurements the carbon coating of the crystals was removed. The Raman measurements were carried out by accumulation of two scans, each with an acquisition time of 600 s at the microscope magnification 100 × ; the minimum lateral and depth resolution ~1 µm, and an estimated analytical spot size of ~3–5 µm. The deconvolution of the recorded spectra was done in the range of 3300–3800 cm^{-1} applying the FITYK-1.3.1 program for data processing and nonlinear curve fitting (Wojdyr 2010), after subtracting a linear background. Low-intense wide bands with Raman shifts below 3400 cm^{-1} (~1–4% relative) were assigned to luminescence, or trace Al or B supplementing deficient Si at the T site (Nishio-Hamane et al. 2014; Kutzschbach et al. 2016, 2021). They were finally subtracted from the spectrum during the calculation of integral intensities of the O–H stretching vibration bands. To evaluate a value of the $^{VOH}I_{YAlZAlZAl} / (^{VOH}I_{YZZ} + {}^{WOH}I_{YYY})$ parameter, component bands with their band positions, full-widths at half maximum (FWHM), and integrated intensities were determined by fitting of an input model with Gaussian function band shapes applying the Levenberg–Marquardt fitting method (Levenberg 1944; Marquardt 1963). Spectral position, height and FWHM of each anticipated band was matched to minimize the difference between the empirical spectrum and the theoretical spectrum designated as the sum of intensities of the anticipated bands. As intense bands with Raman shift < 3600 cm^{-1} related to OH vibration modes with decreasing wavenumber become wider and wider, they were deconvoluted with increasing anticipated FWHM of 16–24 cm^{-1} in case of the band around 3580–3600 cm^{-1}, 18–24 cm^{-1} for that ~3550–3560 cm^{-1}, and 20–45 cm^{-1} for that located < 3500 cm^{-1}, depending on the height of the anticipated band. Less intense bands with Raman shift > 3600 cm^{-1} are more sharp if they are better defined in the spectrum. Therefore, the spectral range 3600–3800 cm^{-1} was deconvoluted with component bands with FWHM, which are generally at 10–40 cm^{-1} depending on the band shape.

Orientation of the tourmaline crystal sections

The studies of the orientation of the crystal sections of the tourmaline samples used for EPMA + SREF + RS investigations were performed with the use of a high-resolution ZEISS AURIGA 60 electron microscope coupled with the Brucker EBSD eFLASH HR+ detector. The tests were carried out using an electron beam with energy of 10 keV and a current close to 8 nA. The processing of the results was performed using the ESPRIT ver. 2.1 software. The investigations were carried out on tourmaline crystals not covered with a carbon layer. The surface of the examined tourmaline crystals was prepared similar as for the preparation of microprobe thin sections (final polishing was performed using a diamond suspension of 1 µm grain diameter). Prior to the electron backscatter diffraction (EBSD) examination, the samples were additionally polished for 2 h using a vibrating polisher and a diamond suspension of ¼ µm grain diameter. Finally, a selected area of tourmaline surface in each sample was framed with a copper tape for the purpose of more effective electron removal.

The EBSD orientation measurements were performed on varying tourmaline areas from ~20 × 20 µm up to of ~690 × 550 µm; a single EBSD map was recorded from the 1.77 × 1.77 µm area during 160 ms. The sample surface was tilted 70° relative to the electron beam, while the detector tilt angle was 1.6°. The distance between the detector and the examined tourmaline surface was 16.55 mm. The orientation of the studied tourmaline cross-section was calculated after the statistical processing of the orientation of the EBSD maps, which was presented using the Euler angles (φ, θ, ψ) in the Landau and Lifschitz (1976) notation. The slope of the surface of the examined tourmaline surface with respect to the **z** crystallographic axis of this mineral determines the nutation angle (θ).

Results

General remarks

The most important refined structural data of the studied tourmalines, (this study; Ertl et al. 2009, 2010, 2013)

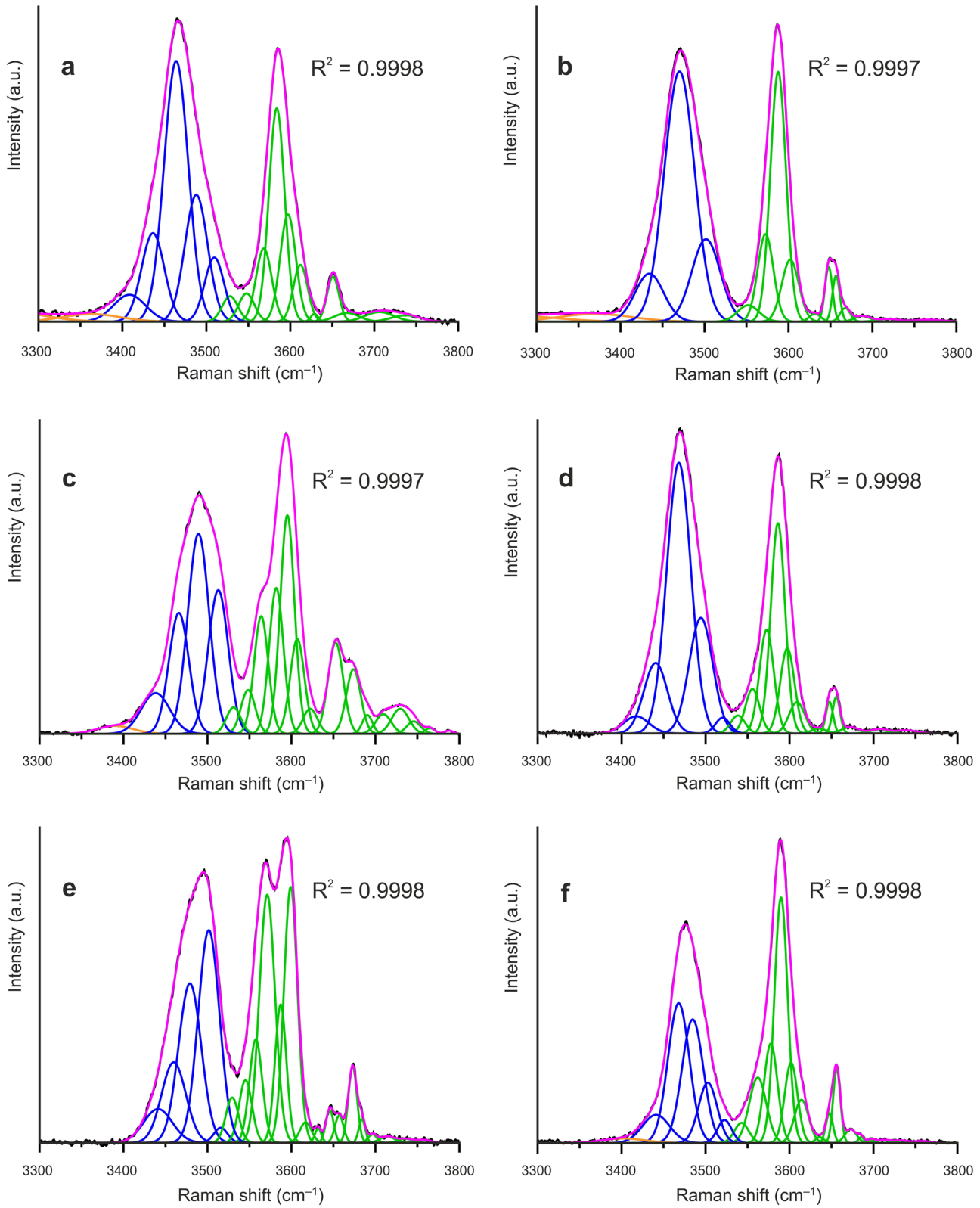

Fig. 1 Raman spectra of the studied tourmalines deconvoluted into component bands: a) SS4, b) MOZ24, c) BUX, d) WOLP, e) P2c, f) P2r. Note: black – measured spectrum, orange – bands not correlating with the O–H stretching vibrations (explanation in the text), blue – bands of ^{V}OH groups bonded to the ^{Y}Al^{Z}Al^{Z}Al triplet, green – bands of all remaining ^{V}OH groups bonded to Y^{2}+^{Z}Al^{Z}Al and ^{Y}Li^{Z}Al^{Z}Al triplets and ^{W}OH groups, violet – fitted model. Abbreviations: R – correlation coefficient between recorded and deconvoluted spectrum

are presented in Table 3. Complete refined data (CIF) are included into the ESM 1. In case of the previously studied crystals, the current results are similar differing usually in 1–2 SD range, although the investigations were done on different crystal fragments. In ESM 2, Table S1, are presented quantitative parameters of deconvolution of O–H stretching vibration modes in Raman spectra of the tourmalines from Figs. 1 and 2, along with a basic interpretation of the revealed component bands. Detailed results referring to each of the studied tourmaline crystal are presented below. We do not discuss the assignments of the component bands in detail. The assignments are usually made based on one of two models that use (1) short-range (local) arrangements around the ^{V}OH and ^{W}OH groups (e.g., Gonzalez-Carreño et al. 1988; Hoang et al. 2011; Skogby et al. 2012; Zhao et al. 2012; Fantini et al. 2014; Berryman et al. 2016; Kutzschbach et al. 2016, 2021; Mercurio et al. 2018; Bronzova et al. 2019), or (2) site-symmetry analysis, which leads to the assumption that H atoms of the ^{V}OH groups are related by rotation around the threefold axis and collectively participate in a single phonon mode. As a result, the energy of the ^{V}O–H stretching band should be influenced by local cation arrangements associated with all three ^{V}OH groups bound to all cations of the octahedral cluster, which can be represented as $^{V}(OH)_3$-[YZZ–YZZ–YZZ] (Watenphul et al. 2016; Bosi et al. 2016; Kutzschbach et al. 2021). We use the short-range arrangement model in our band interpretation, the merits of which are explained by Pieczka et al. (2020). We would therefore like to emphasize that this model, in contrast to the model by Watenphul et al. (2016), offers the possibility of determining a value of the additional compositional parameter $^{VOH}I_{YAlZAlZAl}$ / ($^{VOH}I_{YZZ}$ + $^{WOH}I_{YYY}$) relatively precisely with absolute error < 0.01 and SD ~0.005. This will be done by deconvolution the O–H stretching vibration modes, which can be used in the formula calculation process leading to the estimation of Li and OH with high accuracy. Since the Y-site occupants in (Al,Li)-bearing tourmalines are limited to Al, Li and a divalent cation, three intense bands which may occur in the OH stretching vibration range are related in the model to the ^{V}OH groups bonded to Al^{3+}, Y^{2+} and Li^{+} with increasing energy. Each of the bands can be deconvoluted into several component bands due to the influence of cations, which occupy the X site ($\square^{0+}$, Na^{+}, K^{+}, Ca^{2+}), the T site (Si^{4+}, B^{3+}, Al^{3+}), and indirectly also by the influence of anions at the W sites (OH^{-}, F^{-}, O^{2-}).

In contrast, the model of Watenphul et al. (2016) requires an interpretation based on the chemistry of the entire octahedral cluster $^{V}(OH)_3$-[YZZ–YZZ–YZZ]. For such a model, the mentioned population of cations at the Y site leads to a maximum of 10 cluster arrangements for Z = Al:

1. $^{V}(OH)_3$-[^{Y}Li^{Z}Al^{Z}Al–^{Y}Li^{Z}Al^{Z}Al–^{Y}Li^{Z}Al^{Z}Al]
2. $^{V}(OH)_3$-[^{Y}Li^{Z}Al^{Z}Al–^{Y}Li^{Z}Al^{Z}Al–Y^{2+} ^{Z}Al^{Z}Al]
3. $^{V}(OH)_3$-[^{Y}Li^{Z}Al^{Z}Al–^{Y}Li^{Z}Al^{Z}Al–^{Y}Al^{Z}Al^{Z}Al]
4. $^{V}(OH)_3$-[^{Y}Li^{Z}Al^{Z}Al–Y^{2+} ^{Z}Al^{Z}Al–Y^{2+} ^{Z}Al^{Z}Al]
5. $^{V}(OH)_3$-[^{Y}Li^{Z}Al^{Z}Al–Y^{2+} ^{Z}Al^{Z}Al–^{Y}Al^{Z}Al^{Z}Al]
6. $^{V}(OH)_3$-[^{Y}Li^{Z}Al^{Z}Al–^{Y}Al^{Z}Al^{Z}Al–^{Y}Al^{Z}Al^{Z}Al]
7. $^{V}(OH)_3$-[Y^{2+} ^{Z}Al^{Z}Al–Y^{2+} ^{Z}Al^{Z}Al–Y^{2+} ^{Z}Al^{Z}Al]
8. $^{V}(OH)_3$-[Y^{2+} ^{Z}Al^{Z}Al–Y^{2+} ^{Z}Al^{Z}Al–^{Y}Al^{Z}Al^{Z}Al]
9. $^{V}(OH)_3$-[Y^{2+} ^{Z}Al^{Z}Al–^{Y}Al^{Z}Al^{Z}Al–^{Y}Al^{Z}Al^{Z}Al]
10. $^{V}(OH)_3$-[^{Y}Al^{Z}Al^{Z}Al–^{Y}Al^{Z}Al^{Z}Al–^{Y}Al^{Z}Al^{Z}Al]

The arrangements (1), (2) and (4) do not satisfy the requirements for the bond valence around the W site (Hawthorne 1996, 2016; Bosi 2013) or the electroneutrality of the formula and should therefore not be present in the tourmaline structure. The remaining arrangements show that the three mentioned bands in the O–H stretching vibration range can also be deconvoluted into several (maximum 7) component bands, which may be additionally multiplied by the influence of the cations at the X and T sites and the anions at the W site, as shown above. In that model, however, each component band assigned to one of the seven possible arrangements presented is usually related to two or three different cations at the Y-site triplet or exclusively to cations of only one atomic type. Consequently, each of the three bands in the O–H stretching vibration range is a superposition of a few component bands which correspond to 2–3 arrangements of the cluster $^{V}(OH)_3$-[YZZ–YZZ–YZZ] with different Al, Li, and Y^{2+} contents. This does not offer any possibility, on the basis of the spectrum interpretation, to evaluate with a high degree of accuracy additional compositional parameters, including the mentioned ratio of $^{VOH}I_{YAlZAlZAl}$ / ($^{VOH}I_{YZZ}$ + $^{WOH}I_{YYY}$), that could be used in the calculation formula method. The results of the Li evaluation in Zn-bearing fluor-elbaite using the two models were briefly compared by Pieczka et al. (2020). They found significantly larger differences between Li contents, which were evaluated based on the deconvolution of the Raman spectrum and which were optimized based on SREF data using the model of Watenphul et al. (2016). The problem raised therefore excludes this model from our evaluation.

An interesting study by Kutzschbach et al. (2021) on tetrahedral boron in synthetic Al-rich tourmaline using both models, i.e., the model of short-range ordering around ^{V}OH and ^{W}OH and the model by Watenphul et al. (2016), shows a strong correlation between the tetrahedral boron content and the summed relative intensity of all OH stretch bands in the 3300–3430 cm^{-1} range. However, the authors noted certain differences in the results through applications of the two models. They received a good match for most assignments in the synthetic high-$^{[4]}$B tourmalines and the natural B-free Al-tourmalines in Watenphul et al. (2016), e.g., for the configuration $\square$-AlAlAl–AlAlAl–AlAlAl$^{(Si)}$, but for the synthetitic elbaitic tourmaline the ^{W}OH bands occurred at

Table 3 Refined structural data of the studied tourmalines

	SS4	MOZ24	BUX	WOLP	P2c	P2r	P3c	P3r
R_1	1.22	1.14	1.87	1.14	1.67	1.77	1.67	1.22
a^* (Å)	15.8111(4)	15.818(2)		15.819(2)				
a (Å)	15.8274(2)	15.8259(2)	15.8303(2)	15.8148(1)	15.8898(1)	15.8530(2)	15.9040(1)	15.8430(1)
c^* (Å)	7.0892(4)	7.095(1)		7.094(1)				
c (Å)	7.0999(1)	7.0965(1)	7.0965(1)	7.0983(1)	7.1190(1)	7.1021(1)	7.1247(1)	7.1035(1)
V^* (Å^3)				1537.4(4)				
V (Å^3)	1540.29(3)	1539.25(3)	1540.12(5)	1537.48(3)	1556.63(3)	1545.76(5)	1560.67(3)	1544.11(3)
^{X}s.s.* (e$^-$)	7.83	7.13		5.48				
^{X}s.s. (e$^-$)	7.61(9)	6.80(9)	9.43(12)	5.73(9)	8.33(13)	7.86(12)	9.32(13)	7.24(10)
^{Y}s.s.* (e$^-$)	27.05	30.46		29.14				
^{Y}s.s. (e$^-$)	26.73(15)	27.69(12)	30.12(21)	29.49(12)	38.76(21)	28.50(18)	38.64(21)	25.98(15)
^{T}s.s.* (e$^-$)	13.655	13.993		13.762				
^{T}s.s. (e$^-$)	13.73(4)	13.82(4)	13.48(6)	13.762(42)	13.64(6)	13.75(6)	13.66(6)	13.76(4)
^{W}s.s. (e$^-$)	8.46	8.46		8.26				
^{W}s.s.* (e$^-$)	8.57(6)	8.44(6)	8.56(14)	8.27(5)	8.59(11)	8.73(9)	8.87(12)	8.66(7)
<X–O >* (Å)	2.667(1)	2.673(1)		2.677(2)				
<X–O >(Å)	2.670(2)	2.674(2)	2.666(2)	2.679(2)	2.678(2)	2.672(2)	2.675(2)	2.672(2)
<Y–O> *(Å)	1.992(1)	1.989(1)		1.982(1)				
<Y–O> (Å)	1.994(1)	1.990(1)	2.002(2)	1.980(1)	2.024(2)	2.005(2)	2.032(2)	2.001(1)
<Z–O >* (Å)	1.9040(7)	1.9061(5)		1.907(1)				
<Z–O >(Å)	1.9066(9)	1.9066(8)	1.9067(11)	1.9075(6)	1.9080(13)	1.9070(11)	1.9083(13)	1.9071(9)
<B–O>* (Å)	1.373(1)	1.374(1)		1.374(1)				
<B–O>(Å)	1.374(2)	1.375(1)	1.374(2)	1.374(1)	1.374(2)	1.375(2)	1.375(2)	1.375(2)
<T–O> * (Å)	1.6157(6)	1.6172(5)		1.618(1)				
<T–O> (Å)	1.6178(7)	1.6177(6)	1.6148(10)	1.6177(7)	1.6189(11)	1.6184(10)	1.6201(11)	1.6180(8)

*data from Ertl et al. (2009, 2010, 2013) given in Table 2. Estimated standard deviations are given in parentheses

20–60 cm^{-1} lower wavenumbers compared to the results of Watenphul et al. (2016). According to these authors, the reason of the decreased Raman shifts of the bands might be high amounts of trivalent B substituting for Si at the tetrahedral site.

Applying the short-range arrangement model for our studies together with the characteristic band assignments (Gonzalez-Carreño et al. 1988; Hoang et al. 2011; Skogby et al. 2012; Zhao et al. 2012; Fantini et al. 2014; Berryman et al. 2016; Kutzschbach et al. 2016, 2021; Mercurio et al. 2018; Bronzova et al. 2019), the only criterion for the deconvolution of the spectra in our studies was a high correlation coefficient (close to 100%) between the deconvoluted output spectrum and the primary empirical spectrum for each of the tourmalines examined.

Elbaite SS4 from the Himalaya Mine, San Diego County, California

Pale pink elbaite SS4 was studied and described along with six other tourmaline crystals from the same locality by Ertl et al. (2010). H_2O, Li_2O and B_2O_3 in the tourmaline were determined in the original studies by SIMS as 3.67(1), 1.68(2) and 12.91(8) wt%, respectively. The crystal-chemical formula of the tourmaline (ESM 2, Table S2, analysis 1), $(Na_{0.53}\square_{0.37}Ca_{0.10})_{\Sigma1}(Al_{1.80}Li_{1.05}Mn_{0.02}\square_{0.13})_{\Sigma3}Al_6(BO_3)_3(Si_{5.77}B_{0.23}O_{18})(OH)_3(OH_{0.54}F_{0.46})$, was normalized on 31 (O, OH, F) anions based on H_2O, Li_2O and B_2O_3 amounts optimized to 3.41, 1.68 and 12.04 wt% on the basis of the refined crystal structure (Ertl et al. 2010).

The refinement performed on a single crystal of our sample from SS4 exhibited parameters, which are close to the values presented in the original paper (Table 3). The refined ^{T}s.s. and <T–O> m.b.l. indicate that some boron, with or without small amounts of Al, also occupies the Si position (T site). The crystal chemical formula (based on EPMA + SREF), calculated on the basis of 31 (O, OH, F) anions and a complete occupation of the Y-site triplet, with H_2O, Li_2O and B_2O_3 matching the refined values of ^{Y}s.s. and <T–O> m.b.l. is: $(Na_{0.523}\square_{0.373}Ca_{0.100}K_{0.003})_{\Sigma1}(Al_{1.732}Li_{1.249}Mn_{0.019})_{\Sigma3}Al_6(BO_3)_3(Si_{5.822}B_{0.130}Al_{0.048}O_{18})(OH)_3(OH_{0.481}F_{0.488}O_{0.031})_{\Sigma1}$ (ESM 2, Table S2, analysis 2). This formula indicates ^{T}s.s. = 13.80 e$^-$ and <Y–O> m.b.l. = 1.991 Å [calculated on the basis of effective ionic radii by Shannon (1976)], within ±

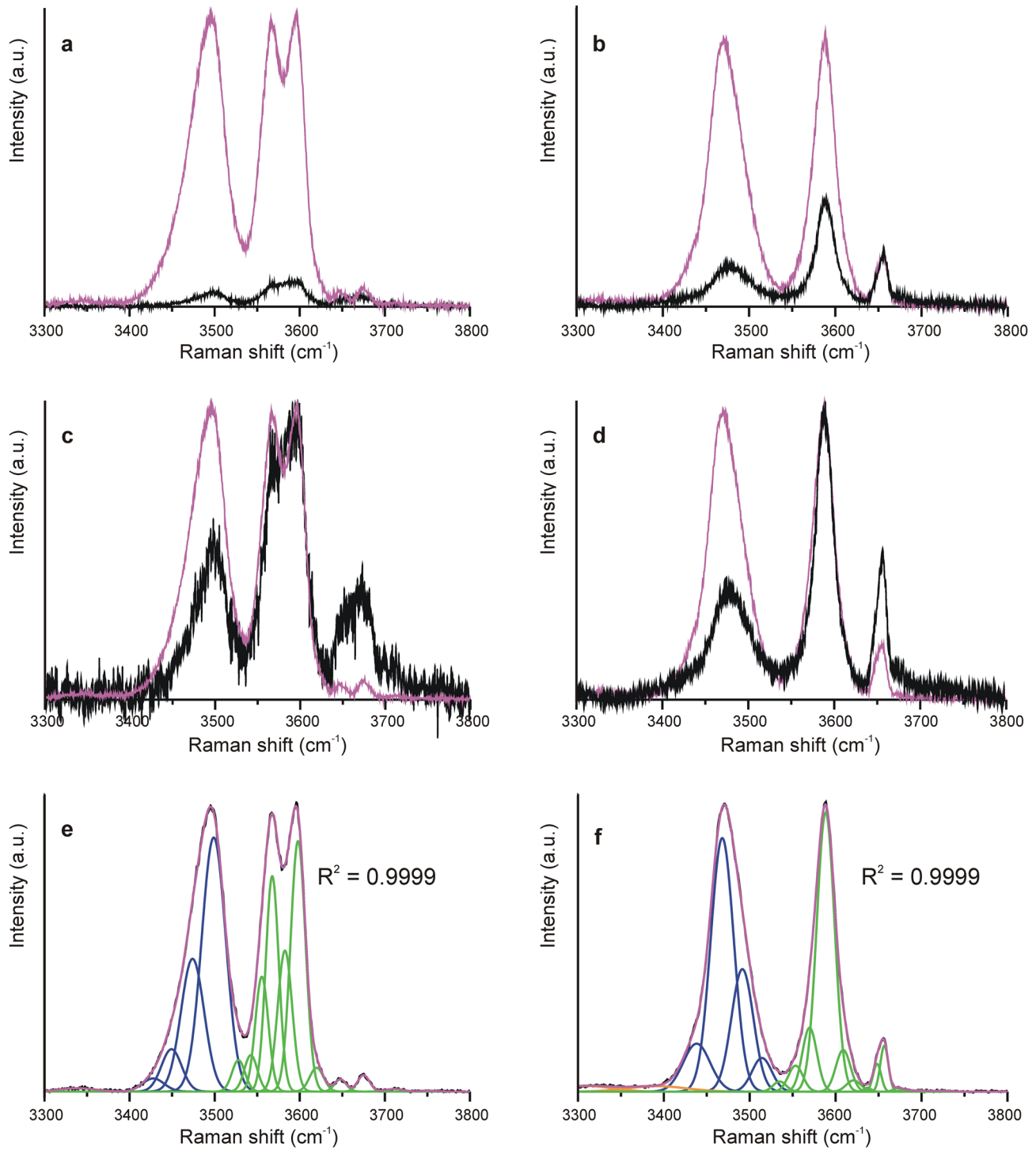

Fig. 2 Raman spectra of O–H stretching vibrations of (Al,Li)-bearing tourmaline sample P3. Orientations: violet – $\parallel$ **c;** black – $\perp$ **c.** Note: (a) core; (b) rim; (c) same spectra as (a), but the scale (the highest peak) of the spectrum $\perp$ **c** was adjusted to the highest peak of the spectrum $\parallel$ **c;** (d) same spectra as (b), but the scale of the spectrum $\perp$ **c** was adjusted to the highest peak of the spectrum $\parallel$ **c;** (e-f) deconvolution of the O–H stretching vibration range of the spectra into component bands; colors and symbols as in Fig. 1

2 SD in agreement with the refined values. The calculated values of Li_2O, H_2O and B_2O_3 are 2.01, 3.38 and 11.75 wt%, respectively. Among the amounts, Li_2O is significantly higher than 1.68(2) wt% determined by SIMS (Ertl et al. 2010). This suggests that the Y-site triplet is not fully occupied as was concluded by Ertl et al. (2010). The recalculated

formula considering a not fully occupied Y-site triplet is: $(Na_{0.525}\square_{0.371}Ca_{0.101}K_{0.003})_{\Sigma1}(Al_{1.775}Li_{1.062}Mn_{0.019}\square_{0.144})_{\Sigma3}Al_6(BO_3)_3(Si_{5.845}B_{0.119}Al_{0.036}O_{18})(OH)_3(OH_{0.510}F_{0.490})$ (ESM 2, Table S2, analysis 3). Such tourmaline composition requires 1.70, 3.40 and 11.66 wt% Li_2O, B_2O_3 and H_2O, respectively, in which these amounts, except for B_2O_3, are almost identical with the values of these components evaluated by Ertl et al. (2010). We conclude that both presented EPMA + SREF formulae of the SS4 sample classify this tourmaline as elbaite (Henry et al. 2011). The X site is dominated by Na, the Y site by Al + Li, and the W site by OH. However, both compositions are close to the mid-member in the elbaite – fluor-elbaite solid solution.

The deconvolution of the O–H stretching vibration range 3300–3800 cm^{-1} in Raman spectrum of the SS4 tourmaline revealed a value of the $^{VOH}I_{YAlZAlZAl}$ / ($^{VOH}I_{YZZ}$ + $^{WOH}I_{YYY}$) parameter of ~0.5946 (Fig. 1a; ESM 2, Table S1). This value, used as a constraint on the ^{Y}Al / $^{V+W}$OH ratio in the EPMA + RS formula calculation, led to the following crystal-chemical formula with fully occupied Y sites: $(Na_{0.530}\square_{0.366}Ca_{0.102}K_{0.003})_{\Sigma1}(Al_{1.863}Li_{1.118}Mn_{0.019})_{\Sigma3}Al_6(BO_3)_3(Si_{5.892}B_{0.096}Al_{0.012}O_{18})(OH)_3(F_{0.494}O_{0.373}OH_{0.133})$, for which the calculated site-scattering values and <Y–O> and <T–O> m.b.l. are presented in ESM 2, Table S2 (analysis 4). The too high calculated electron density for the Y-site triplet together with the too small <Y–O> m.b.l. in relation to the refined values is a simple consequence of too low evaluated Li and OH contents and raised content of ^{Y}Al. The differences of the Li and OH contents between the EPMA + RS and the EPMA + SREF formulae are relatively large (Table 4). The model with a not fully occupied Y-site triplet leads to a very similar EPMA + RS formula: $(Na_{0.530}\square_{0.365}Ca_{0.102}K_{0.003})_{\Sigma1}(Al_{1.878}Li_{1.039}Mn_{0.019}\square_{0.064})_{\Sigma3}Al_6(BO_3)_3(Si_{5.900}B_{0.094}Al_{0.006}O_{18})(OH)_3(F_{0.494}O_{0.347}OH_{0.158})$, also with elevated Y-site scattering and shortened <Y–O> m.b.l. (ESM 2, Table S2, analysis 5). For this formula, the differences of the Li and OH contents in relation to the contents estimated on the basis of similarly normalized EPMA + SREF results are -0.023 and -0.352 apfu, which correspond to differences of -0.05 and -0.37 wt% Li_2O and H_2O. In consequence to this differences, $^{W}O^{2-}$ is significantly overestimated in both evaluated EPMA + RS formulae, and due to ^{W}(OH + F) > ^{W}O and ^{W}F > ^{W}OH, both presented EPMA + RS formulae of SS4 tourmaline would classify it incorrectly as fluor-elbaite.

Table 4 Differences Δ in the Li_2O (Li) and H_2O (OH) contents evaluated by the EPMA + RS and EPMA + SREF methods

Sample	$\Delta(^{Y}Al / ^{V+W}OH)^1$	ΔLi_2O^2 (wt%)	ΔH_2O^3 (wt%)	ΔLi^4 (apfu)	ΔOH^5 (apfu)
SS4	0.097	-0.233	-0.374	-0.131	-0.348
MOZ24	0.071	-0.176	-0.281	-0.010	-0.260
BUX	-0.001	-0.004	-0.006	0.002	0.006
WOLP	0.018	-0.042	-0.077	-0.023	-0.068
P2c	0.050	-0.138	-0.237	-0.080	-0.219
P2r	0.007	-0.020	-0.035	-0.011	-0.032
P3c ($\|\|$ **c**)	0.066	-0.195	-0.264	-0.113	-0.240
P3r ($\|\|$ **c**)	0.123	-0.365	-0.489	-0.203	-0.431
Zn[6]	0.032	-0.106	-0.142	-0.065	-0.132

[1] $\Delta(^{Y}Al/^{V+W}OH) = (^{Y}Al/^{V+W}OH)_{EPMA+RS} - (^{Y}Al/^{V+W}OH)_{EPMA+SREF}$

[2] $\Delta Li_2O = Li_2O_{EPMA+RS} - Li_2O_{EPMA+SREF}$

[3] $\Delta H_2O = H_2O_{EPMA+RS} - H_2O_{EPMA+SREF}$

[4] $\Delta Li = Li_{EPMA+RS} - Li_{EPMA+SREF}$

[5] $\Delta OH = OH_{EPMA+RS} - OH_{EPMA+SREF}$

[6] data for Zn-bearing fluor-elbaite was calculated by using formulae from Pieczka et al. (2020)

Cu-bearing elbaite MOZ24 from the Alto Ligonha plateau, Mozambique

Violet-pink tourmaline MOZ24 was studied and described together with other Cu-bearing tourmalines from Mozambique and Brazil by Ertl et al. (2013). For this tourmaline (ESM 2, Table S2, analysis 6), these authors proposed the following formula: $(Na_{0.63}\square_{0.36}Ca_{0.01})_{\Sigma1}(Al_{2.12}Li_{0.87}Cu_{0.01})_{\Sigma3}Al_6(BO_3)_3(Si_{5.96}Al_{0.04}O_{18})(OH)_3(OH_{0.54}F_{0.46})$ with the Y-site triplet completely occupied by cations. The refined structural parameters are presented in Table 3. The shortened <T–O> m.b.l. = 1.6172(5) Å may indicate small amounts of B at the T site. However, the formula of this tourmaline was originally explained with a stoichiometric B content and small amount of tetrahedrally-coordinated Al.

In Table 3 we present structural parameters of our refinement of this tourmaline sample. Note that the <Y–O> and <T–O> m.b.l. are almost identical, while ^{Y}s.s. and ^{T}s.s. are different to the Y- and T-site electron densities indicated by the Ertl et al. (2013) formula [30.46 and 13.99 e^-, respectively; ESM 2, Table S2, analysis 6]. This seems to be a consequence of the aforementioned assumption referring to the T-site occupancy and the procedures of Li_2O and H_2O calculations by accepting completely occupied Y sites and totals of OH + F = 4 anions pfu. Because of similar refined X, Y, Z, B and T mean-bond lengths we have to expect similar site scattering values in both refinements. Therefore we propose a new formula, considering ^{Y}s.s. and <T–O> m.b.l., with recalculated B_2O_3, Li_2O and H_2O contents for a full occupancy of the Y sites. As a result, the following formula of this tourmaline was obtained: $(Na_{0.615}\square_{0.372}Ca_{0.013})_{\Sigma1}(Al_{1.832}Li_{1.154}Cu_{0.014})_{\Sigma3}Al_6(BO_3)_3(Si_{5.779}B_{0.152}Al_{0.069}O_{18})(OH)_3(OH_{0.453}F_{0.447}O_{0.099})$ (ESM 2, Table S2, analysis 7). It is very close to the

crystal-chemical formula obtained on the basis of our EPMA + SREF results at the same calculating criterions: $(Na_{0.593}\square_{0.397}Ca_{0.011})_{\Sigma1}(Al_{1.839}Li_{1.150}Cu_{0.012})_{\Sigma3}Al_6(BO_3)_3(Si_{5.812}B_{0.136}Al_{0.052}O_{18})(OH)_3(OH_{0.548}F_{0.338}O_{0.115})$ (ESM 2, Table S2, analysis 8). Both the original formula of the tourmaline sample by Ertl et al. (2013) and the new proposed formula as well as the formula optimized on the basis of our SREF results correspond to an intermediate member of the elbaite – fluor-elbaite solid solution with a dominant elbaite end-member because of predominant occupants at the X (= Na), Y (= Al, Li) and W site (= OH).

The deconvolutions of O–H stretching vibrations in the range 3300–3800 cm^{-1} in Raman spectrum of the tourmaline revealed a value of the $^{VOH}I_{YAlZAlZAl}$ / ($^{VOH}I_{YZZ}$ + $^{WOH}I_{YYY}$) parameter close to 0.5896 (Fig. 1b, ESM 2, Table S1). Calculation of the EPMA + RS formula with completely occupied Y sites, normalized to 31(O, OH, F) apfu with the constraint of the ^{Y}Al/(^{V}OH + ^{W}OH) ratio to the spectral parameter led to the formula: $(Na_{0.598}\square_{0.391}Ca_{0.011})_{\Sigma1}(Al_{1.938}Li_{1.050}Cu_{0.012})_{\Sigma3}Al_6(BO_3)_3(Si_{5.864}B_{0.112}Al_{0.024}O_{18})(OH)_3(OH_{0.287}F_{0.341}O_{0.372})$ (ESM 2, Table S2, analysis 9). Similar to the elbaite (SS4) from the Himalaya Mine, a too high value of ^{Y}s.s. by ~1 e^- was calculated on the basis of the EPMA + RS evaluated formula. The shortened <Y–O> m.b.l. and raised ^{Y}Al prove too small amounts of Li and OH estimated on the basis of the spectral parameter in relation to the EPMA + SREF optimized contents. Consequently, relatively high differences occur between the EPMA + RS and EPMA + SREF evaluated contents of Li and OH (Table 4), and the EPMA + RS formula would classify tourmaline MOZ24 incorrectly as fluor-elbaite.

Mushroom elbaite BUX from Momeik, Myanmar

The refined structural parameters of elbaite sample BUX are presented in Table 3. The decreased ^{T}s.s. and shortened <T–O> m.b.l. indicate, as previously, a deficiency of silicon and some tetrahedrally-coordinated boron. EPMA analysis supplemented with B_2O_3, Li_2O and H_2O data, matching the calculated ^{Y}s.s. and <T–O> m.b.l. to the refined values considering the assumption of a completely occupied Y-site triplet corresponds to the following EPMA + SREF formula: $(Na_{0.706}\square_{0.245}Ca_{0.048})_{\Sigma1}(Al_{1.715}Li_{1.105}Mn_{0.168}Fe_{0.012})_{\Sigma3}Al_6(BO_3)_3(Si_{5.792}B_{0.208}O_{18})(OH)_3(OH_{0.796}O_{0.204})$ (ESM 2, Table S2, analysis 10). The $^{VOH}I_{YAlZAlZAl}$ / ($^{VOH}I_{YZZ}$ + $^{WOH}I_{YYY}$) parameter evaluated by the deconvolution of the O–H stretching vibration modes in the Raman shift range of 3300–3800 cm^{-1} was designated at ~0.4507 (Fig. 1c, ESM 2, Table S1). The convergence of the spectral parameter with ^{Y}Al/(^{V}OH + ^{W}OH) ratio derived from the calculated EPMA + RS formula was achieved for B_2O_3, Li_2O and H_2O amounts equal to 11.84, 1.75 and 3.63 wt%, respectively, which lead to the EMPA + RS evaluated formula: $(Na_{0.705}\square_{0.246}Ca_{0.048})_{\Sigma1}(Al_{1.713}Li_{1.107}Mn_{0.168}Fe_{0.012})_{\Sigma3}Al_6(BO_3)_3(Si_{5.790}B_{0.210}O_{18})(OH)_3(OH_{0.802}O_{0.198})$ (ESM 2, Table S2, analysis 11). Both the EPMA + SREF as well as EPMA + RS evaluated formulae indicate almost identical X, Y, T and W site-scattering values and <Y–O> and <T–O> m.b.l. comparable with the refined data. Differences between the contents of Li and OH derived from the formulae are insignificant (Table 4). Thus, for this tourmaline sample a perfect agreement between formulae derived from the EPMA + RS and EPMA + SREF data was achieved. Both formulae classify this tourmaline as elbaite due to the same arguments as those mentioned previously.

Rossmanite WOLP from Wolkenburg, Saxony, Germany

Tourmalines from a pegmatite at Wolkenburg, Saxony, Germany, were studied by Ertl et al. (2009) and characterized as members of the fluor-elbaite – rossmanite series due to varying occupation of the X, Y and W sites. For sample WOLP with H_2O, Li_2O and B_2O_3 amounts determined by SIMS with 3.57, 1.14 and 11.70 wt%, respectively, the EMPA + SIMS + SREF results gave the following crystal-chemical formula normalized to 31 (O, OH, F) anions: $(\square_{0.51}Na_{0.48}Ca_{0.01})_{\Sigma1}(Al_{2.02}Li_{0.71}Mn_{0.03}\square_{0.24})_{\Sigma3}Al_6(BO_3)_3(Si_{5.69}B_{0.14}Al_{0.17}O_{18})(OH)_3(OH_{0.70}F_{0.26}O_{0.04})$ (ESM 2, Table S2, analysis 12). Site scattering values for sites occupied by more then one occupant and the refined mean bond lengths are presented in Table 3. Based on the chemical and structural data this tourmaline was assigned to a complex solid solution of rossmanite (51 mol.%), fluor-elbaite (13 mol.%) and olenite (27 mol.%) end-members (Ertl et al. 2009).

Another fragment of the crystal was characterized chemically and structurally by us. The data presented in Table 3 and ESM 2, Table S2, analysis 13, are similar to the chemistry and refined parameters by Ertl et al. (2009). As the previous tourmalines, the decreased ^{T}s.s. and <T–O> m.b.l. require additionally to Si either B or Al + B. The EPMA + SREF formula normalized to 31 (O, OH, F) anions together with the assumption of a fully occupied Y-site triplet, matching the calculated ^{Y}s.s and <T–O> m.b.l. with the refined values and supplemented by optimized B_2O_3, Li_2O and H_2O contents is $(\square_{0.557}Na_{0.443})_{\Sigma1}(Al_{2.029}Li_{0.962}Mn_{0.009})_{\Sigma3}Al_6(BO_3)_3(Si_{5.773}B_{0.154}Al_{0.073}O_{18})(OH)_3(OH_{0.513}O_{0.281}F_{0.205})$ (ESM 2, Table S2, analysis 13). The deconvolution of the spectral range of O–H stretching vibration modes 3300–3800 cm^{-1} in the Raman spectrum of this tourmaline sample allowed an evaluation of the $^{VOH}I_{YAlZAlZAl}$ / ($^{VOH}I_{YZZ}$ + $^{WOH}I_{YYY}$) parameter at ~0.5953 (Fig. 1d, ESM 2, Table S1), and calculation of the EPMA + RS formula with the constraint of the ^{Y}Al/(^{V}OH + ^{W}OH) ratio to the value of the spectral

parameter: $(\square_{0.556}Na_{0.444})_{\Sigma1}(Al_{2.051}Li_{0.939}Mn_{0.009})_{\Sigma3}Al_6(BO_3)_3(Si_{5.792}B_{0.131}Al_{0.077}O_{18})(OH)_3(OH_{0.446}O_{0.348}F_{0.206})$. The formulae require 1.50–1.55 wt% Li_2O and 3.33–3.40 wt% H_2O (ESM 2, Table S2, analyses 13 and 14), and are characterized by differences in Li and OH contents between the EPMA + RS and EPMA + SREF evaluated formulae presented in Table 4. However, the Li_2O amount analyzed by SIMS exhibits only 1.14 wt% and H_2O 3.57 wt% (Ertl et al. 2009); both values are different compared with the evaluated contents, under the assumption of a complete occupancy of the Y-site triplet. Therefore, we also checked the possibility of the presence of vacancies in the Y-site triplet. The resulted respective EPMA + SREF and EPMA + RS formulae are: $(\square_{0.555}Na_{0.445})_{\Sigma1}(Al_{2.086}Li_{0.714}Mn_{0.009}\square_{0.191})_{\Sigma3}Al_6(BO_3)_3(Si_{5.802}B_{0.141}Al_{0.057}O_{18})(OH)_3(OH_{0.557}O_{0.236}F_{0.206})$, and $(\square_{0.554}Na_{0.446})_{\Sigma1}(Al_{2.102}Li_{0.683}Mn_{0.010}\square_{0.206})_{\Sigma3}Al_6(BO_3)_3(Si_{5.810}B_{0.137}Al_{0.052}O_{18})(OH)_3(OH_{0.530}O_{0.263}F_{0.206})$ (ESM 2, Table S2, analyses 15 and 16). These formulae present calculated Li_2O and H_2O contents with 1.09–1.14 and 3.40–3.43 wt%, which are in better agreement with the respective SIMS measured amounts given in the original paper by Ertl et al. (2009). There are also smaller differences of the Li and OH contents between those EPMA + RS and EPMA + SREF evaluated formulae: -0.030 and -0.027 apfu, which correspond to differences of the respective oxides with -0.05 and -0.03 wt%. In the tourmaline-supergroup minerals nomenclature system by Henry et al. (2011), due to the vacancy-dominant X site, the Y-site occupancy with Al >> Li and the W-site occupancy predominated by OH, all evaluated formulae classify this tourmaline as rossmanite.

Bicolour elbaite – fluor-elbaite crystals from Piława Górna, Poland

This is one of main varieties of coloured (Al,Li)-tourmalines from the Julianna pegmatitic system at Piława Górna crystallized in a late stage of the system consolidation, forming crystals up to 10 cm long and a few cm in diameter. Cores of the crystals are usually pale green with a yellowish tint, whereas the rims show a pinkish to raspberry red colour. Two crystals of the tourmaline were studied: P2 in an accidental section, and P3 in the section $\|\mathbf{c}$. ESM 2, Table S2, analyses 17 and 21 present chemical compositions of the core of both samples (P2, P3), and analyses 19 and 23 of the rim of both samples. Refined structural characteristics of the tourmalines are presented in Table 3. Decreased ^{T}s.s. and <T–O> m.b.l., especially in the crystal P2, indicate that some B, with or without small amounts of Al, also occupies the Si position. Therefore the EPMA + SREF formulae of the core and rim tourmaline P2 and core tourmaline P3 were normalized for 31 (O, OH, F) anions, whereas the rim tourmaline P3 was normalized for 14.5 (O, OH, F) anions with constraints on the calculated <T–O> m.b.l. and ^{Y}s.s (ESM 2, Table S2, analyses 17, 19, 21, 23). The EPMA + RS formulae were normalized to 31 (O, OH, F) anions for the P2 core and rim tourmaline (ESM 2, Table S2, analyses 18, 20), and to 14.5 (O, OH, F) anions for the core and rim tourmaline of the P3 crystal (ESM 2, Table S2, analyses 22, 24) with the constraint on the value of the $^{VOH}I_{YAlZAlZA}l$ / ($^{VOH}I_{YZZ}$ + $^{WOH}I_{YYY}$) parameter, respectively ~0.4553, 0.4717, 0.4617 and 0.5725, derived from Raman spectra of the tourmalines (Figs. 1e-f, 2e-f; ESM 2, Tables S1 and S2). The optimized EMPA + SREF formulae of these tourmalines are:

P2c: $(Na_{0.648}Ca_{0.016}K_{0.005}\square_{0.332})_{\Sigma1}(Al_{1.416}Li_{0.881}Mn_{0.554}Fe^{2+}_{0.149})_{\Sigma3}Al_6(BO_3)_3(Si_{5.937}B_{0.058}Al_{0.005}O_{18})(OH)_3(OH_{0.491}F_{0.354}O_{0.155})$
P2r: $(Na_{0.557}Ca_{0.082}\square_{0.360})_{\Sigma1}(Al_{1.601}Li_{1.241}Mn_{0.147}Fe^{2+}_{0.011})_{\Sigma3}Al_6(BO_3)_3(Si_{5.936}B_{0.064}O_{18})(OH)_3(F_{0.535}OH_{0.417}O_{0.017})$
P3c: $(Na_{0.733}Ca_{0.046}K_{0.004}\square_{0.217})_{\Sigma1}(Al_{1.272}Li_{0.964}Mn_{0.648}Fe^{2+}_{0.117})_{\Sigma3}Al_6(BO_3)_3(Si_{5.997}B_{0.003}O_{18})(OH)_3(F_{0.649}OH_{0.217}O_{0.134})$
P3r: $(Na_{0.574}Ca_{0.051}K_{0.003}\square_{0.373})_{\Sigma1}(Al_{1.633}Li_{1.311}Mn_{0.056})_{\Sigma3}Al_6(BO_3)_3(Si_{6.000}O_{18})(OH)_3(OH_{0.634}F_{0.366})$

The calculated electron densities at the X, Y, T and W sites, and <Y–O> and <T–O> m.b.l. are presented in ESM 2, Table S2; they are in excellent agreement with the refined values of these samples, presented in Table 3. The only exception seems to be tourmaline P3r for which a small difference between the refined and calculated ^{Y}s.s. appears due to the limitation of the formula optimization by OH+F = 4 apfu. The calculated EMPA + RS formulae for these tourmalines are as follows:

P2c: $(Na_{0.654}Ca_{0.016}K_{0.005}\square_{0.326})_{\Sigma1}(Al_{1.490}Li_{0.801}Mn_{0.559}Fe^{2+}_{0.150})_{\Sigma3}Al_6(BO_3)_3(Si_{5.993}B_{0.007}O_{18})(OH)_3(O_{0.374}F_{0.357}OH_{0.269})$
P2r: $(Na_{0.558}Ca_{0.082}\square_{0.360})_{\Sigma1}(Al_{1.611}Li_{1.230}Mn_{0.147}Fe^{2+}_{0.011})_{\Sigma3}Al_6(BO_3)_3(Si_{5.944}B_{0.056}O_{18})(OH)_3(F_{0.536}OH_{0.446}O_{0.048})$
P3c: $(Na_{0.743}Ca_{0.047}K_{0.004}\square_{0.206})_{\Sigma1}(Al_{1.375}Li_{0.851}Mn_{0.657}Fe^{2+}_{0.117})_{\Sigma3}Al_6(BO_3)_3(Si_{6.000}O_{18})[(OH)_{2.997}O_{0.023}]_{\Sigma3}(F_{0.658}O_{0.342})$
P3r: $(Na_{0.589}Ca_{0.053}K_{0.003}\square_{0.356})_{\Sigma1}(Al_{1.834}Li_{1.109}Mn_{0.057})_{\Sigma3}Al_6(BO_3)_3(Si_{6.000}O_{18})(OH)_3(O_{0.422}F_{0.375}OH_{0.203})$

Comparing the respective EPMA + SREF and EPMA + RS formulae, differences between the Li and OH contents evaluated by application of both calculation methods are obvious. More, Li and OH contents estimated by the EPMA + RS method are always smaller than on the basis of EMPA + SREF, as was already observed for the previously investigated samples (Table 4). The EPMA + SREF formulae (due to the X site predominated by Na, Y site by Al + Li, and W site by OH) classify the core P2 tourmaline and rim

P3 tourmaline as elbaite, and the rim tourmaline P2 and core tourmaline P3 as fluor-elbaite due to F + OH > O and F > OH. However, due to an underestimated content of ^{W}OH and overestimated content of ^{W}O the EPMA + RS formulae classify some tourmalines erroneously as fluor-elbaite.

The presented examples for the determination of crystal chemical formulae of (Al,Li,OH)-bearing tourmalines based on EPMA and deconvolution of O–H-stretching vibration modes in their Raman spectra, which were recorded on non-oriented crystal sections, show different results in relation to the formulae optimized on the basis of EPMA + SREF results. This suggests that the EPMA + RS technique of the formula calculation is influenced by the effect of the crystal section orientation on which Raman spectrum was collected.

Discussion

The influence of the crystal section orientation on the Li and OH estimation

In Table 5 we compare the Li_2O contents estimated by a variety of methods:

(i) based on EPMA + SREF data with constraints for the calculated Y-site electron density and <T–O> m.b.l. to the refined values,
(ii) based on EPMA + RS data with the constraint for the calculated ^{Y}Al / $^{V+W}$OH ratio to the $^{VOH}I_{YAlZAlZAl}$ / ($^{VOH}I_{YZZ}$ + $^{WOH}I_{YYY}$) parameter evaluated by the deconvolution of O–H stretching modes in Raman spectrum,
(iii) by using the equation proposed by Pesquera et al. (2016).

Co-variations between the estimated EPMA + SREF Li_2O contents (1) and the contents estimated by application of the two other methods (2, 3) are presented in Fig. 3. At first sight, the Li_2O contents estimated based on EPMA + RS and those calculated from the equation of Pesquera et al. (2016) seem to be similar to the Li_2O contents estimated on the basis of EPMA + SREF data: depending on the crystal examined, either method (2) or (3) is in better agreement to the Li_2O content, which was optimized based on EPMA + SREF. Methods (2) and (3) produce slightly different average values and SDs, respectively 1.57(28) and 1.69(24) wt% versus 1.71(30) Li_2O wt% (optimized value based on EPMA + SREF data). Note, however, four important features in the co-variations:

(i) all EPMA + RS evaluated Li_2O contents are smaller than the respective contents evaluated by EPMA + SREF. This is in contrast to the contents evaluated by the Pesquera et al. (2016) equation;
(ii) the difference between the estimated Li_2O content based on the Pesquera et al. (2016) equation and the EPMA + SREF content may also increase in the presence of significant amounts of an atypical tourmaline component (e.g., Zn in Zn-bearing fluor-elbaite as mentioned before);
(iii) the estimation of the Li_2O content by applying the equation described by Pesquera et al. (2016) leads to relatively large differences in case of not-fully occupied Y sites;
(iv) by comparing the Li_2O contents evaluated on the basis of EPMA + RS data and those evaluated from EMPA + SREF data, and by comparing the differences between the EPMA + RS evaluated $^{VOH}I_{YAlZAlZAl}$ / ($^{VOH}I_{YZZ}$ + $^{WOH}I_{YYY}$) parameter and the value of the ^{Y}Al / $^{V+W}$OH ratio derived from the EPMA + SREF formula, it is obvious that larger differences (Δ) in the Li_2O (Li) and H_2O (OH) contents correspond to larger differences in the ^{Y}Al / $^{V+W}$OH parameter (Table 4).

Table 5 Li_2O contents (wt%) in the studied (Al,Li)-bearing tourmalines estimated by the three described methods

Sample	EPMA + SREF	EPMA + RS[1]	Pesquera et al. (2016)
SS4	2.013	1.780	1.835
MOZ24	1.849	1.674	1.777
BUX	1.749	1.753	1.665
WOLP	1.545	1.503	1.596
P2c	1.390	1.252	1.320
P2r	1.991	1.971	1.873
P3c	1.503	1.308	1.406
P3r	2.073	1.708	2.037
Zn	1.261	1.159[4]	1.986[2]
SS4[3]	1.704	1.651	1.835
WOLP[3]	1.140	1.090	1.596

[1]EPMA + RS contents effected by the section orientation

[2]without ZnO = 5.70 wt%

[3]Li_2O contents estimated for the case with not-fully occupied Y sites

[4]data for Zn-bearing fluor-elbaite (Zn) was calculated by using formulae from Pieczka et al. (2020)

The correlations between the differences Δ of Li, OH, and ^{Y}Al / $^{V+W}$OH are presented in Fig. 4 (in wt% and atomic scale). A characteristic feature of these relationships is their straight line, which points approximately '0', indicating that at Δ(^{Y}Al / $^{V+W}$OH) close to 0 the estimated contents of Li_2O (Li) and H_2O (OH) show only minimal inaccuracies. The differences

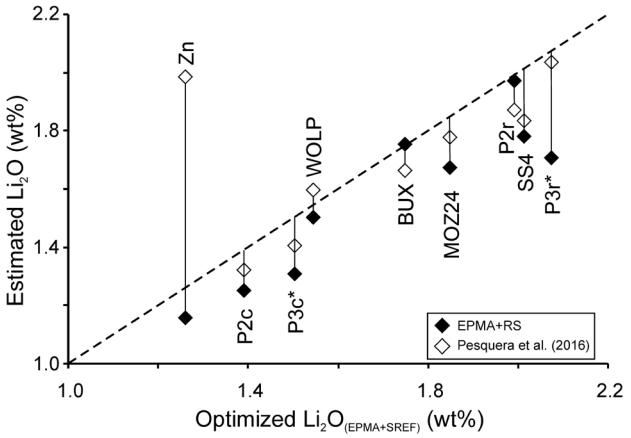

Fig. 3 A co-variation of the Li_2O contents estimated with the discussed EPMA + RS technique (different orientations), and on basis of the statistical equation of Pesquera et al. (2016) versus the Li_2O contents optimized based on EPMA + SREF data. Thin vertical tie-lines indicate differences in the estimated Li_2O contents by the two mentioned methods in relation to those estimated from EPMA + SREF data. Dashed line: perfect agreement between the EPMA + RS (or the statistical technique of Pesquera et al. 2016) with EPMA + SREF. Star: EPMA + RS Li_2O contents evaluated from a Raman spectrum collected in the section ∥ **c** sample P3. Zn: Zn-bearing fluor-elbaite (Pieczka et al. 2020)

ΔLi_2O and ΔH_2O are correlated with $\Delta(^{Y}Al$ / $^{V+W}OH)$ by the relationships: y = -2.6729x – 0.0033 (R^2 = 0.975) and y = -3.7796x – 0.0153 (R^2 = 0.992), and the differences ΔLi and ΔOH correlate with $\Delta(^{Y}Al$ / $^{V+W}OH)$ by the relationships: y = -1.5337x – 0.0014 (R^2 = 0.971) and y = -3.4887x – 0.0118 (R^2 = 0.991). In turn, the relationships between ΔH_2O and ΔLi_2O on a weight percent scale and between ΔOH and ΔLi on an atomic scale are: y = 1.3826x – 0.0149 (R^2 = 0.973) and y = 2.2146x – 0.0136 (R^2 = 0.967), respectively. All of these relationships show excellent correlations with a coefficient R close to 1 (0.983–0.996; Fig. 4). Small values of the constant parameters in these relationships, in the range 0.003–0.015 wt% for the oxides and 0.001–0.014 apfu, indicate that Li_2O (Li) and H_2O (OH) evaluated by the constraint of the ^{Y}Al / ^{V+W}OH ratio of the calculated formula to the $^{VOH}I_{YAlZAlZAl}$ / ($^{VOH}I_{YZZ}$ + $^{WOH}I_{YYY}$) parameter derived from the Raman spectrum should have a high degree of accuracy.

The straight-line relationships from Fig. 4 clearly show that the orientation of the crystal section is, at least, one of the first-order effects that affect the $^{VOH}I_{YAlZAlZAl}$ / ($^{VOH}I_{YZZ}$ + $^{WOH}I_{YYY}$) parameter and thus also the adapted Li_2O (Li) and H_2O (OH) contents in the EPMA + RS evaluated (Al,Li)-bearing tourmaline formula. The orientation effects are clearly visible in Raman spectra of O–H stretching vibration modes, which were recorded for the core and rim in tourmaline crystal P3 on the sections perpendicular and parallel to **c** (Fig. 2a-b). The intensity of the O–H stretching modes in the spectrum collected on the section ∥ **c** is several to ~10 times higher than in the spectrum collected on the section ⊥ **c**. In addition, the intensities of individual bands change disproportionately, and as a result, the band with a Raman shift < 3500 cm^{-1}, related to ^{V}OH group bound to the $^{Y}Al^{Z}Al^{Z}Al$ triplet, disappears faster than those bands that correspond to the $Y^{2+}\,^{Z}Al^{Z}Al$ and $^{Y}Li^{Z}Al^{Z}Al$ triplets occurring in the Raman shift range of 3500–3600 cm^{-1} (Fig. 2c-d). Bands corresponding to ^{W}O–H vibrations (> 3600 cm^{-1}) are relatively more intense when they are collected on the section ⊥ **c** than ∥ **c**. Such a development of OH stretching vibration modes in an (Al,Li)-bearing tourmaline spectrum as a function of the crystal section orientation is undoubtedly a result of the different crystallographic orientation of ^{W}O–H and ^{V}O–H bonds in the structure and the excitation of the modes modified by surrounding cations from the Y and Z sites by a laser beam to different degrees depending on the direction of the beam. The idealized ^{V}O–H bond for each possible ^{V}OH-$Y^{Z}Al^{Z}Al$ configuration (Y = Li, Y^{2+}, Al) must be included in the **a**-**c** plane and form with the **c** direction an angle dependent on the Y-site occupant. In case of the most regular ^{V}OH-$^{Y}Al^{Z}Al^{Z}Al$ configuration (Y = Al) showing the highest symmetry in charge distribution, the O–H vector should be aligned to the **c** axis at a high angle; for the two remaining clusters ^{V}OH-$Y^{2+}\,^{Z}Al^{Z}Al$ and ^{V}OH-$^{Y}Li^{Z}Al^{Z}Al$ the respective angles should be smaller due to higher asymmetry in the charge distribution. In consequence, a laser beam aligned perpendicularly to the section (but in a high degree parallel to the O–H bonds) excites the ^{V}O–H stretching modes observed in the spectrum as ^{V}O–H bands with high intensities. Gonzales-Carreño et al. (1988) expected for (Mn,Fe)-bearing elbaites angles close to 40–50° between the **c** axis and the direction of the ^{V}O–H bonds. However, Gatta et al. (2012) using single-crystal neutron and X-ray diffraction structure refinements found only an angle of 5.4(4)° between both directions and provided no explanation for the differences in relation to the angles expected from a polarized Raman spectrum by Gonzales-Carreño et al. (1988). In the section ⊥ **c** the laser beam is aligned parallel to the **c** axis, i.e., under high angles in relation to the direction of the ^{V}OH bonds, thus they are only slightly excited. As a result, the intensities of the ^{V}OH bonds decrease distinctly when the spectrum is recorded from diagonal sections drawing towards ⊥ **c.** In case of ^{W}O–H bond participating in the formation of more compositionally differentiated clusters ^{W}OH-YYY (Y = Li, Y^{2+}, Al) it may be expected that the bonds in the most regular ^{W}OH-AlAlAl and ^{W}OH-$Y^{2+}Y^{2+}Y^{2+}$ clusters will be excited with the highest rates for sections ⊥ **c**, because the ^{W}O–H vector corresponds to the **c** direction, i.e., coincides with the direction of the laser beam. For the remaining five YYY clusters, the ^{W}O–H vectors should be aligned diagonally in relation to the **c** axis under angles dependent on the YYY cation combinations. This explains

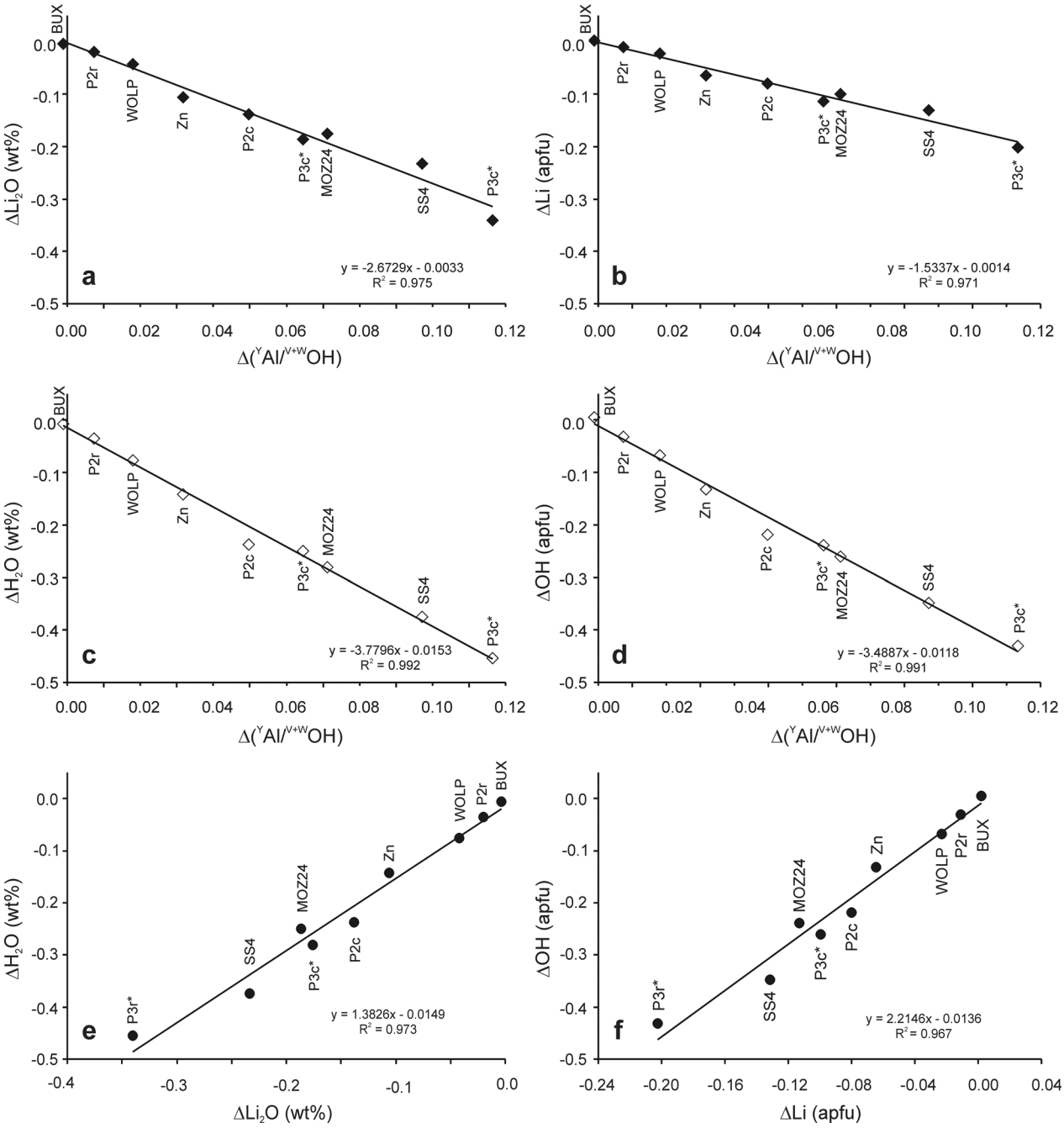

Fig. 4 Covariations of observed differences Δ evaluated through the EPMA + RS(0) and EPMA + SREF formula calculations: (a-b) between the ^{Y}Al / $^{V+W}$OH parameter, and the Li_2O and Li contents on the weight percent and atomic scale, respectively; (c-d) between the ^{Y}Al / $^{V+W}$OH parameter, and the ΔH_2O and ΔOH contents on the weight percent and atomic scale, respectively; (e) between ΔLi_2O and ΔH_2O contents on weight percent scale; (f) between ΔLi and ΔOH contents on atomic scale. The abbreviation EPMA + RS(0) denotes that the tourmaline formula was calculated based on the EPMA analysis considering the ratio ^{Y}Al / $^{V+W}$OH = $^{VOH}I_{YAlZAlZAl}$ / ($^{VOH}I_{YZZ}$ + $^{WOH}I_{YYY}$) derived by the deconvolution of O–H stretching vibrations in the Raman spectrum (not considering the effect of the crystal surface orientation, i.e., without iteration procedure eliminating this effect)

the slower loss of the relative intensity of the ^{W}OH bonds in relation to the ^{V}OH bonds in sections close to $\perp$ **c** as it is shown in Fig. 2c, d. In sections close to $\parallel$ **c** direction, the laser beam is perpendicular or almost perpendicular to the ^{W}O–H vectors, and the respective bonds are excited with small rates.

The orientation of the crystal sections of the examined tourmalines, on which the Raman spectra were recorded, is

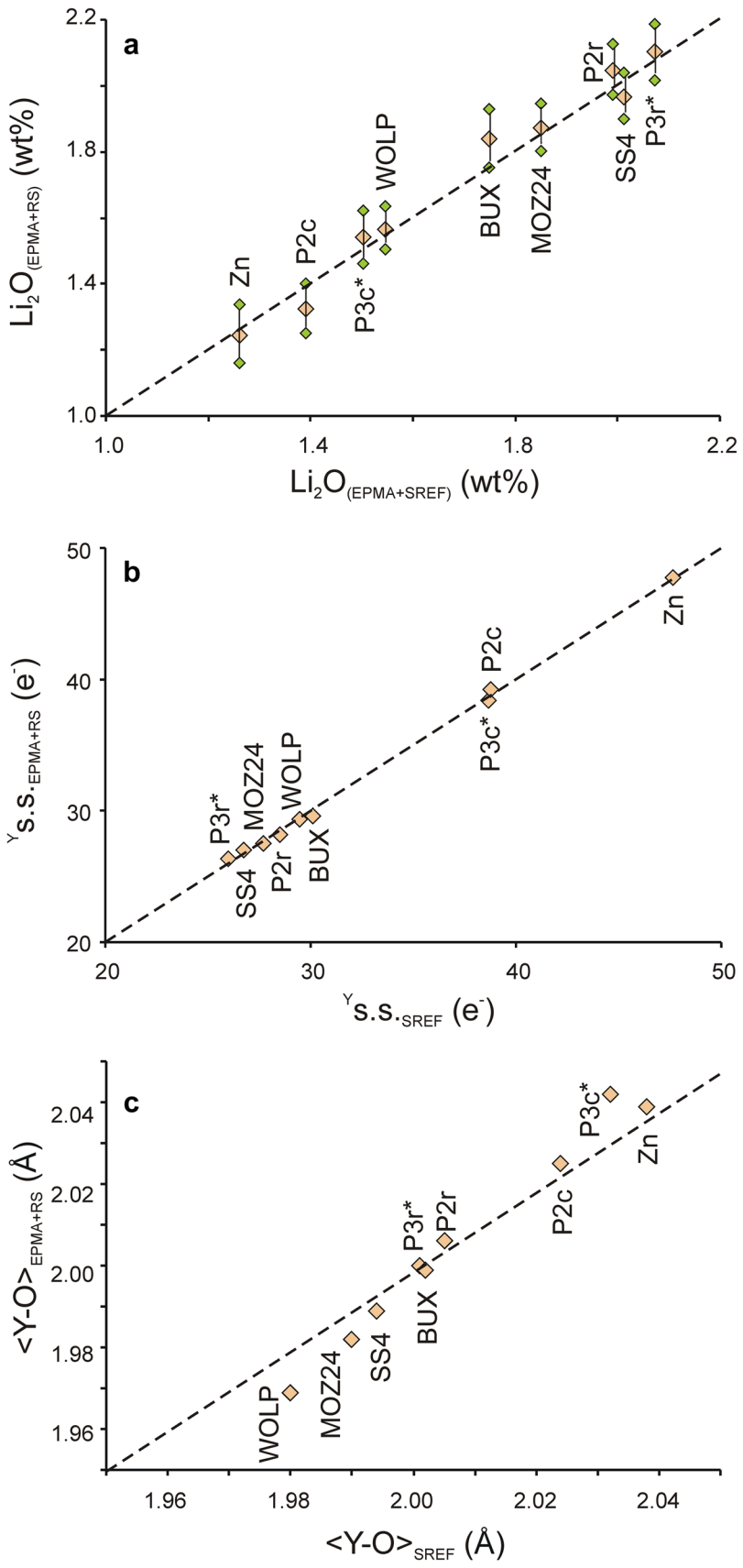

Fig. 5 Covariations between the SREF optimized: (**a**) Li_2O content, (**b**) total scattering at the Y-site triplet, (**c**) <Y–O> mean bond length, and the respective data from the EPMA + RS evaluated formulae after correcting the influence of the crystal section orientation by using the described iteration procedure. Dashed lines in the plots denote 1:1 relation between the respective variables. Green diamonds – data evaluated based on ^{Y}Al / $^{V+W}$OH value iterated in two successive stages RS_n and RS_{n+1}, orange diamonds – data evaluated for average value of ^{Y}Al / $^{V+W}$OH

shown in Table 6 by specifying the nutation θ angle which is determined by statistical processing of the orientation of the recorded EBSD maps. The nutation angle corresponds to an angle between the crystallographic axis **c** and the normal to the sample surface. The compilation of the data presented in Table 4 and the measured orientations from Table 6 clearly shows that the smallest differences in ΔLi and ΔOH between the EPMA + RS and EPMA + SREF evaluated Li and OH contents apply to Raman spectra, which were recorded on sections $\perp$ **c** (BUX), while the highest differences were recorded for sections $\parallel$ **c** (P3c and P3r, SS4, and also WOLP).

Table 6 Orientation of crystal sections of the studied (Al,Li)-tourmalines (angle between the crystallographic axis **c** and the normal to the sample surface)

Crystal (section)	Number of patterns	Min (°)	Max (°)	Mean (°)	SD (°)
SS4	429	88.2	92.7	89.7	0.6
MOZ24	948	45.1	50.7	48.0	0.8
BUX	62663	0	4.7	2.3	0.7
WOLP	2076	86.3	88.5	87.4	0.3
P2c	1777	43.2	44.4	43.7	0.2
P2r	946	38.4	43.1	40.5	0.5
P3c ($\perp$ **c**)	1438	4.1	5.8	4.7	0.2
P3r ($\perp$ **c**)	869	3.0	4.3	3.5	0.3
P3c ($\parallel$ **c**)	1769	85.1	89.9	86.2	0.3
P3r ($\parallel$ **c**)	1211	86.9	88.9	87.9	0.4

SD standard deviation (1-sigma error)

A method of correcting the influence of orientation of the crystal section

The presented results clearly show an influence of the orientation (of the crystal section) on the Li and OH contents, which were evaluated using the Raman spectrum on the basis of parameter $^{VOH}I_{YAlZAlZAl} / (^{VOH}I_{YZZ} + {}^{WOH}I_{YYY})$. This is due to the fact that, depending on the crystal section orientation, not all $^{V+W}$OH groups are excited by the laser beam in the same degree. This fact shows that an earlier assumption that "the O–H stretching vibration range reflects quantitatively the chemical bonds of all OH groups from the V and W sites together with all bonded octahedral cations, …" (Pieczka et al. 2020) is generally not entirely correct. For sections that are more parallel to the **c** axis, the component $^{VOH}I_{YZZ}$ in the denominator of the fraction decreases and the resulting increase in the value of the fraction consequently leads to an underestimation of Li and OH and an overestimation of ^{Y}Al during the EPMA + RS formula calculation (this is the case for almost all tourmalines studied in this work). The reason is the alignment of O–H vectors with respect to the **c**-axis as discussed above. This remark suggests the fundamental question of whether O–H stretching vibrations are well suited for the evaluation of the Li and OH content in (Al,Li)-bearing tourmalines and the determination of their crystal chemical formulae.

The answer seems to be in the affirmative. Figure 4 shows that for some of the investigated crystals the Raman spectrum was collected on an almost 'ideal' section for which the difference $\Delta(^{Y}Al / {}^{V+W}OH)$ between the value of the parameter derived from the Raman spectrum and that of the value derived from the EPMA + SREF data was very small, e.g., ~0.02 (P2r, WOLP; Table 4) or even close to zero (BUX). This indicates that such an 'ideal' section could be found by detailed examination, for example, of several sections of the same (Al,Li)-bearing tourmaline that were cut at different angles with respect to the **c** direction. However, the EBSD measurements of the crystal section orientation carried out (Table 6) cannot meet this expectation, since, for example, the best-adapted EPMA + RS and EPMA + SREF formulae for the BUX crystal with almost $\Delta(^{Y}Al / {}^{V+W}OH) = 0$, and where ΔLi and ΔOH parameters are estimated for the section almost $\perp$ **c**, while the P2r and WOLP formulae with only slightly larger differences $\Delta(^{Y}Al / {}^{V+W}OH)$, ΔLi and ΔOH were calculated from Raman spectra collected for a diagonal section and almost $\parallel$ **c**. Our conclusion contained in the last sentence of the previous subsection therefore makes it necessary to develop a method for estimating an accurate Li and OH content in which the effects of orientation are only minor.

As mentioned earlier ΔLi, ΔOH and $\Delta(^{Y}Al / {}^{V+W}OH)$ variables are connected with each other by three following linear regression equations:

$$\Delta Li = -1.5337 \cdot \Delta\left(^{Y}Al/^{V+W}OH\right) - 0.0014 \ \left(R^2 = 0.971\right) \quad (1)$$

$$\Delta OH = -3.4887 \cdot \Delta\left(^{Y}Al/^{V+W}OH\right) - 0.0018 \ \left(R^2 = 0.991\right) \quad (2)$$

$$\Delta OH = 2.2146 \cdot \Delta Li - 0.0136 \ \left(R^2 = 0.967\right) \quad (3)$$

An expansion of the equations with $\Delta(^{Y}Al / {}^{V+W}OH) = (^{Y}Al / {}^{V+W}OH)_{RS} - (^{Y}Al / {}^{V+W}OH)_{SREF}$, $\Delta Li = Li_{RS} - Li_{SREF}$, and $\Delta OH = OH_{RS} - OH_{SREF}$, leads to the following version of the system:

$$1.5337 \cdot \left(^{Y}Al/^{V+W}OH\right)_{SRFF} + Li_{SRFF} = 1.5337 \cdot \left(^{Y}Al/^{V+W}OH\right)_{RS} + Li_{RS} + 0.0014 \quad (4)$$

$$3.4887 \cdot \left(^{Y}Al/^{V+W}OH\right)_{SRFF} + OH_{SRFF} = 3.4887 \cdot \left(^{Y}Al/^{V+W}OH\right)_{RS} + OH_{RS} + 0.0118 \quad (5)$$

$$2.2146 \cdot Li_{SRFF} - OH_{SRFF} = 2.2146 \cdot Li_{RS} - OH_{RS} - 0.0136 \quad (6)$$

This linear system of equations is fulfilled for the Li_{RS} and OH_{RS} adaptation $(^{Y}Al / {}^{V+W}OH)_{RS}$ if the later variable tends towards the value of $(^{Y}Al / {}^{V+W}OH)_{SREF}$. Since Li_{RS}, OH_{RS} and $(^{Y}Al / {}^{V+W}OH)_{RS}$ are influenced by orientation effects, it is only possible to determine values of the variables in subsequent iterations in order to bring them to the real values identified with Li_{SREF}, OH_{SREF} and $(^{Y}Al / {}^{V+W}OH)_{SREF}$ that have been optimized on the basis of the results of the X-ray structure refinement. Hence, the system of linear equations can be given as follows:

$$1.5337 \cdot \left(^{Y}Al/{}^{V+W}OH\right)_{RS(n+1)} + Li_{RS(n+1)} = 1.5337 \cdot \left(^{Y}Al/{}^{V+W}OH\right)_{RS(n)} + Li_{RS(n)} + 0.0014 \quad (7)$$

$$3.4887 \cdot \left(^{Y}Al/{}^{V+W}OH\right)_{RS(n+1)} + OH_{RS(n+1)} = 3.4887 \cdot \left(^{Y}Al/{}^{V+W}OH\right)_{RS(n)} + OH_{RS(n)} + 0.0118 \quad (8)$$

$$2.2146 \cdot Li_{RS(n+1)} - OH_{RS(n+1)} = 2.2146 \cdot Li_{RS(n)} - OH_{RS(n)} - 0.0136, \quad (9)$$

where $(^{Y}Al / {}^{V+W}OH)_{RS(n)}$, $Li_{RS(n)}$ and $OH_{RS(n)}$ are values of the parameters in n^{th} iteration cycle, $(^{Y}Al / {}^{V+W}OH)_{RS(n+1)}$, $Li_{RS(n+1)}$ and $OH_{RS(n+1)}$ the parameters obtained in $(n + 1)^{th}$ iteration cycle, beginning from the influenced Li and OH contents and the $(^{Y}Al / {}^{V+W}OH)$ parameter, evaluated directly from EPMA and the deconvoluted RS spectrum, for which $n = 0$. In practice, achieving a satisfactory solution requires the need to perform 1–2 (exceptionally 3) iterations in the system of equations and calculate the resulting tourmaline formula each time based on the newly determined value of $^{Y}Al / {}^{V+W}OH$ parameter. As the EPMA + SREF formulae evaluated by us show, the completion of the iteration process should correspond to an iteration cycle in which the sum of the OH_{RS} + F evaluated would be $3.75 < OH_{RS} + F \leq 4$ apfu. Since in each iteration cycle the estimated Li_{RS} and OH_{RS} values are closer to the ideal Li_{SREF} and OH_{SREF} values than the initial $Li_{RS(0)}$ and $OH_{RS(0)}$ values in the primary EPMA + RS (influenced) formula, is a control of the iterated results possible for each level of the formula iteration.

ESM 2, Table S3 shows EPMA + RS formulae that were estimated for the examined tourmaline crystals with an indication of the number of iterations [EPMA + RS(0) - EPMA + RS(3)]; for each crystal, two EPMA + RS formulae are shown that come closest to the EPMA + SREF formula, which was calculated assuming full occupancy of the Y-site triplet, as well as the averaged formula based on the averaged value of $(^{Y}Al / {}^{V+W}OH)$ parameter characteristic for these formulae. In general, the number of iterations (n = 0–3) depends on the initial value of the difference $\Delta(^{Y}Al / {}^{V+W}OH) = (^{Y}Al / {}^{V+W}OH)_{RS(0)} - (^{Y}Al / {}^{V+W}OH)_{SREF}$: sections near $\|\mathbf{c}$ with high $\Delta(^{Y}Al / {}^{V+W}OH)$ values require 2 (3) iterations, diagonal sections 1–2, and for the sections near $\perp \mathbf{c}$ with the lowest $\Delta(^{Y}Al / {}^{V+W}OH)$ values that for $(^{Y}Al / {}^{V+W}OH)_{RS(0)}$ calculated 'influenced' formula may then already match the EPMA + SREF formula. Figure 5a shows the graphical results of the described Li_2O (wt%) evaluation. Although it is possible to select the formula from the two EPMA + RS proposed formulae that best fits the EPMA + SREF results, we recommend using the formula calculated with OH + F in the range of 3.75–4 anions based on the average value of the $^{Y}Al / {}^{V+W}OH$ parameter for 0–1, 1–2 or 2–3 steps of the EPMA + RS formula iteration, since there are often no refined structural data available (this was also the reason for the analysis of the EPMA + RS method). Covariations of the EPMA + RS evaluated ^{Y}s.s. values and <Y–O> m.b.l. with the refined values are shown in Fig. 5b and c.

Analogously, it would also be possible, as in the case of the previously discussed system of linear equations, to create a program that works at the wt% scale, that makes an estimate by iterating successive $(^{Y}Al / {}^{V+W}OH)_{RS(n+1)}$ values and calculation the respective tourmaline formulae with the restriction of the $^{Y}Al / {}^{V+W}OH$ ratio to the $(^{Y}Al / {}^{V+W}OH)_{RS(n+1)}$ value at $3.75 < OH_{RS(n+1)} + F < 4$ apfu leading to similar, albeit slightly different final formulae. The difference is a simple consequence of two independent systems of linear equations that operate on the atomic or percentage scale, which can be used for the EPMA + RS evaluation of the (Al,Li,OH)-bearing tourmaline formula.

Precision of the Li and OH content estimation based on EPMA + RS

ESM 2, Table S4 contains some statistical data that characterize the effects of the calculation of the EPMA + RS tourmaline formula with the assumption of Y = 3 apfu, not affected by the crystal section orientation, obtained by the iteration procedure of the $^{Y}Al / {}^{V+W}OH$ parameter. Each of the calculated EPMA + SREF formulae must be located between two EPMA + RS formulae, which are evaluated for two values of the $^{Y}Al / {}^{V+W}OH$ ratio, in two successive iteration stages RS_n and RS_{n+1}. The values $\Delta Li_{RS} = Li_{RS(n+1)} - Li_{RS(n)}$ and $\Delta OH_{RS} = OH_{RS(n+1)} - OH_{RS(n)}$ therefore indicate the maximum errors in the evaluation of the Li and OH contents, which would occur if the iteration would be terminated in an improper stage. This range must correspond to ~6 SDs, where 1 SD presents a maximum value of the parameter. The statistics of the data for the examined 9 crystals of (Al,Li,OH)-bearing tourmalines show the differences Δ of 0.13–0.18 wt% Li_2O and 0.22–0.28 wt% H_2O with respective average values of 0.16(2) and 0.25(2) wt% and SDs of 0.03(0) and 0.0(4) wt%. On the atomic scale the contents correspond to the ranges 0.08–0.011 Li apfu and 0.20–0.26 OH apfu with respective average values of

0.09(1) and 0.23(2) apfu, and SDs 0.015(2) and 0.038(3). The latter values represent the accuracy of the evaluation of the Li and OH content in OH-bearing (Al,Li)-tourmalines and of the calculation of their formulae by EMPA coupled with deconvolution of O–H stretching vibration modes in their Raman spectra.

Conclusions

We tested the possibility of evaluating Li and OH in (Al,Li,OH)-bearing tourmalines through the deconvolution of O–H stretching vibrations in the range of 3300–3800 cm^{-1} in Raman spectra, which were obtained from randomly oriented sections of 6 pegmatitic (Al,Li)-rich tourmaline crystals which can be assigned to the elbaite, fluor-elbaite and rossmanite species. Based on component band assignments, which are suitable for the model of short-range arrangements around the ^{V}OH and ^{W}OH sites, we have evaluated a quantitative parameter $^{VOH}I_{YAlZAlZAl}$ / ($^{VOH}I_{YZZ}$ + $^{WOH}I_{YYY}$) for each spectrum through the deconvolution of the OH stretching mode. This parameter was used as a constraint on the ^{Y}Al / $^{V+W}$OH ratio during the tourmaline formula calculation process based on the EPMA analysis. The very small inaccuracies of the parameter (<<0.01) ensure a high level of accuracy of the evaluated Li and OH contents.

The comparison of the (EPMA + RS)-evaluated Li and OH contents with the contents optimized on the basis of EPMA + SREF showed an influence of the orientation of the crystal section on the evaluated Li and OH contents, highest for sections $\parallel \mathbf{c}$, and decreasing when approaching towards $\perp \mathbf{c}$. Differences Δ between the (EPMA + RS)- and (EPMA + SREF)-evaluated values of the ^{Y}Al / $^{V+W}$OH parameter and the Li and OH contents are linked by a system of linear relationships. These relationships offer the possibility of eliminating the orientation effect by multilevel (0–3) iteration of the predicted ^{Y}Al / $^{V+W}$OH value and calculation of a new formula in each level up to the evaluated contents $3.75 < OH_{RS} + F \leq 4$ apfu, that comes closest to the contents optimized according to EPMA + SREF. As two solutions are usually possible for the range of OH + F = 3.75–4 anions corresponding to levels 0–1, 1–2 or 2–3, we recommend the average value of the ^{Y}Al / $^{V+W}$OH parameter for the final formula calculation (this procedure corresponds to the lack of structural data and the consequent impossibility of determining the optimized EPMA + SREF formula).

For the average ranges of the evaluated Li and OH values for two successive iteration stages of 0.16(2) wt% Li_2O [0.09(1) Li apfu] and 0.25(2) wt% H_2O [0.23(2) OH anions pfu], the minimum precision of the Li and OH evaluation is 0.03(0) wt% Li_2O [0.015(2) Li apfu] and 0.04(0) wt% H_2O [0.038(3) OH anions pfu]. The comparison of the EPMA + SREF optimized Li_2O contents with the Li_2O contents evaluated according to the described EPMA + RS method on the one hand and the evaluated contents by using the Pesquera et al. (2016) equation on the other hand, gives better results when using the EPMA + RS method. Consequently, the EPMA + RS method reproduces values of some structural parameters quite well, e.g., <Y–O> mean distance or Y site-scattering. The ability to quantitatively determine light elements using the EPMA + RS method makes it comparable to single crystal X-ray diffraction and structure refinement and particularly useful in investigating compositional problems on the micrometer scale, e.g. growth zoning.

Users of the EPMA + RS method of the (Al,Li,OH)-bearing tourmaline formula calculation with estimated Li and OH contents should be aware that the method works similarly as the method of the tourmaline formula optimization, based on EPMA and SREF results, i.e., requires an additional assumption Y = 3 apfu (or Y + Z = 9 apfu). As a result, the estimated Li (Li_2O) and OH (H_2O) contents may differ from the real contents. Therefore, the empirical formula of such tourmaline could be slightly different if the two light components were determined directly, since the formula would be calculated in relation to 31 (O, OH, F) anions without additional assumption and the tourmaline could show Y-site vacancies. Thus, the method can be used when Li_2O and H_2O cannot be determined directly or analyses in a very small crystal area are required. This new method can be applied relatively quickly; all calculations after deconvolution of the recorded Raman spectrum can be performed in a time of ~1 h with a previously prepared Excel program for tourmaline formula calculation, a scientific calculator for solving linear equations or any other tool accessible via the Internet.

Supplementary Information The online version contains supplementary material available at https://doi.org/10.1007/s00710-022-00774-2.

Acknowledgements We thank Martin Kutzschbach and three anonymous experts for their constructive reviews, and Boriana Mihailova for helpful comments on an earlier version of the manuscript. This study was supported by the National Science Centre (Poland) grant 2015/19/B/ST10/01809 and AGH University of Science and Technology grant 16.16.140.315, both to A.P., and in part by the Austrian Science Fund (FWF) project P 31049-N29 to A.E.

References

Berryman EJ, Wunder B, Ertl A, Koch-Müller M, Rhede D, Scheidl K, Giester G, Heinrich W (2016) Influence of the X-site compositionon tourmaline's crystal structure: Investigation of synthetic K-dravite, dravite oxy-uvite, and magnesio-foitite using SREF and Raman spectroscopy. Phys Chem Miner 43:83–102

Bosi F (2013) Bond-valence constraints around the O1 site of tourmaline. Mineral Mag 77:343–351

Bosi F (2018) Tourmaline Crystal Chemistry. Am Mineral 103(2):298–306

Bosi F, Skogby H, Balić-Žunić T (2016) Thermal stability of extended clusters in dravite: a combined EMP SREF and FTIR study. Phys Chem Miner 43:395–407

Bronzova Y, Babushkina M, Frank-Kamenetskaya O, Vereshchagin O, Rozhdestvenskaya I, Zolotarev A (2019) Short-range order in Li-Al tourmalines: IR spectroscopy, X-ray single crystal diffraction analysis and bond valence theory approach. Phys Chem Miner 46:815–825

Dolomanov OV, Bourhis LJ, Gildea RJ, Howard JAK, Puschmann H (2009) *OLEX2*: a complete structure solution refinement and analysis program. J Appl Crystallogr 42:339–341

Dyar MD, Taylor ME, Lutz TM, Francis CA, Guidotti CV, Wise M (1998) Inclusive chemical characterization of tourmaline: Mössbauer study of Fe valence and site occupancy. Am Mineral 83:848–864

Ertl A, Hughes JM, Prowatke S, Rossman GR, London D, Fritz EA (2003) Mn-rich tourmaline from Austria: structure chemistry optical spectra and relations to synthetic solid solutions. Am Mineral 88:1369–1377

Ertl A, Kolitsch U, Meyer H-P, Ludwig T, Lengauer CL, Nasdala L, Tillmanns E (2009) Substitution mechanism in tourmalines in the "fluor-elbaite" – rossmanite series from Wolkenburg Saxony Germany. Neu Jb Mineral Abh 186:51–61

Ertl A, Rossman GR, Hughes JM, London D, Wang Y, O'Leary JA, Dear MD, Prowatke S, Ludwig T, Tillmanns E (2010) Tourmaline of the elbaite-schorl series from the Himalaya Mine Mesa Grande California: A detailed investigation. Am Mineral 95:24–40

Ertl A, Schuster R, Hughes JM, Ludwig T, Meyer H-P, Finger F, Dyar MD, Ruschel K, Rossman GR, Klötzli U, Brandstätter F, Cl L, Tillmanns E (2012) Li-bearing tourmalines in Variscan granitic pegmatites from the Moldanubian nappes Lower Austria. Eur J Mineral 24:695–715

Ertl A, Giester G, Schüssler U, Brätz H, Okrusch M, Tillmanns E, Bank H (2013) Cu- and Mn-bearing tourmalines from Brazil and Mozambique: crystal structures chemistry and correlations. Mineral Petrol 107:265–279

Ertl A, Hughes JM, Prowatke S, Ludwig T, Lengauer CL, Meyer H-P, Giester G, Kolitsch U, Prayer A (2022) Alumino-oxy-rossmanite from pegmatites in Variscan metamorphic rocks from Eibenstein an der Thaya Lower Austria Austria: a new tourmaline that represents the most Al-rich end-member composition. Am Mineral 107(2):157–166

Fantini C, Tavares MC, Krambrock K, Moreira RL, Righi A (2014) Raman and infrared study of hydroxyl sites in natural uvite fluor-uvite magnesio-foitite dravite and elbaite tourmalines. Phys Chem Miner 41:247–254

Gatta GD, Danisi RM, Adamo I, Meven M, Diella V (2012) A single-crystal neutron and X-ray diffraction study of elbaite. Phys Chem Miner 39:577–588

Gonzalez-Carreño T, Fernandez M, Sanz J (1988) Infrared and electron microprobe analysis of tourmalines. Phys Chem Miner 15:452–460

Hawthorne FC (1996) Structural mechanisms for light-element variations in tourmaline. Can Mineral 34:123–132

Hawthorne FC (2016) Short-range atomic arrangements in minerals I: The minerals of the amphibole, tourmaline and pyroxene supergroups. Eur J Mineral 28:513–536

Henry DJ, Novák M, Hawthorne FC, Ertl A, Dutrow BL, Uher P, Pezzotta F (2011) Nomenclature of the tourmaline-supergroup minerals. Am Mineral 96:895–913

Hoang LH, Hien NTM, Chen XB, Minh NV, Yang I-S (2011) Raman spectroscopic study of various types of tourmalines. J Raman Spectrosc 42:1443–1446

Kutzschbach M, Wunder B, Rhede D, Koch-Müller M, Ertl A, Giester G, Heinrich W, Franz G (2016) Tetrahedral boron in natural and synthetic HP/UPH tourmaline: Evidence from Raman spectroscopy EMPA and single-crystal XRD. Am Mineral 101:93–104

Kutzschbach M, Wunder B, Wannhoff I, Wilke FDH, Couffignal F, Rocholl A (2021) Raman spectroscopic quantification of tetrahedral boron in synthetic aluminum-rich tourmaline. Am Mineral 106:872–882

Landau LD, Lifschitz EM (1976) Mechanics, 3rd edn. Pergamon Press, Oxford

Levenberg K (1944) A method for the solution of certain non-linear problems in least squares. Q Appl Math 2:164–168

Marquardt D (1963) An algorithm for least-squares estimation of nonlinear parameters. SIAM J Appl Math 11:431–441

Mercurio M, Rossi M, Izzo F, Cappelletti P, Germinario C, Grifa C, Petrelli M, Vergara A, Langella A (2018) The characterization of natural gemstones using non-invasive FT-IR spectroscopy: New data on tourmalines. Talanta 178:147–159

Nishio-Hamane D, Minakawa T, Yamaura J, Oyama T, Ohnishi M, Shimobayashi N (2014) Adachiite a Si–poor member of the tourmaline supergroup from the Kiura mine Oita Prefecture Japan. J Mineral Petrol Sci 109:74–78

Pesquera A, Gil-Crespo PP, Torres-Ruiz F, Torres-Ruiz J, Roda-Robles E (2016) A multiple regression method for estimating Li in tourmaline from electron microprobe analyses. Mineral Mag 80:1129–1133

Pieczka A, Gołębiowska B, Jeleń P, Włodek A, Szełęg E, Szuszkiewicz A (2018) Towards Zn-dominant tourmaline: a case of Zn-rich fluor-elbaite and elbaite from the Julianna system at Piława Górna Lower Silesia SW Poland. Minerals 8:126

Pieczka A, Ertl A, Gołębiowska B, Jeleń P, Kotowski J, Nejbert K, Stachowicz M, Giester G (2020) Crystal structure and Raman spectroscopic studies of OH stretching vibrations in Zn-rich fluor-elbaite. Am Mineral 105:1622–1630

Pouchou J-L, Pichoir F (1991) Quantitative analysis of homogeneous or stratified microvolumes applying the model "PAP." In: Heinrich KFJ, Newbury DE (eds) Electron Probe Quantitation. Plenum Press, New York, pp 31–75

Roda-Robles E, Simmons W, Pesquera A, Gil-Crespo PP, Nizamoff J, Torres-Ruiz J (2015) Tourmaline as a petrogenetic monitor of the origin and evolution of the Berry-Haveypegmatite (Maine USA). Am Mineral 100:95–109

Shannon RD (1976) Revised effective ionic radii and systematic studies of interatomic distances in halides and chalcogenides. Acta Crystallogr A 32:751–767

Sheldrick GM (2015a) SHELXT – Integrated space-group and crystal-structure determination. Acta Crystallogr A 71:3–8

Sheldrick GM (2015b) Crystal structure refinement with SHELXL. Acta Crystallogr C 71:3–8

Skogby H, Bosi F, Lazor P (2012) Short-range order in tourmaline: a vibrational spectroscopic approach to elbaite. Phys Chem Miner 39:811–816

Sokolov PB, Gorskaya MG, Gordienko VV, Petrova MG, Kretser YL, Frank-Kamenetskii VA (1986) Olenite $Na_{1-x}Al_3Al_6B_3Si_6O_{27}(O, OH)_4$ – a new high-alumina mineral of the tourmaline group. Zap Vses Mineral Obshch 115:119–123 (in Russian)

Szuszkiewicz A, Szełęg E, Pieczka A, Ilnicki S, Nejbert K, Turniak K, Banach M, Łodziński M, Różniak R, Michałowski P (2013) The Julianna pegmatite vein system at the Piława Górna mine Góry Sowie Block SW Poland – preliminary data on geology and descriptive mineralogy. Geol Q 57:467–484

Watenphul A, Burgdorf M, Schlüter J, Horn I, Malcherek T, Mihailova B (2016) Exploring the potential of Raman spectroscopy for crystallochemical analyses of complex hydrous silicates: II Tourmalines. Am Mineral 101:970–985

Wojdyr M (2010) Fityk a general-purpose peak fitting program. J Appl Crystallogr 43:1126–1128

Zhao C, Liao L, Xia Z, Sun X (2012) Temperature-dependent Raman and infrared spectroscopy study on iron-magnesium tourmalines with different Fe content. Vib Spectrosc 62:28–34